



## Monitoring shipping emissions in the German Bight using MAX-DOAS measurements

André Seyler<sup>1</sup>, Folkard Wittrock<sup>1</sup>, Lisa Kattner<sup>1,2</sup>, Barbara Mathieu-Üffing<sup>1,2</sup>,  
Enno Peters<sup>1</sup>, Andreas Richter<sup>1</sup>, Stefan Schmolke<sup>2</sup>, and John P. Burrows<sup>1</sup>

5 <sup>1</sup>Institute of Environmental Physics, University of Bremen, Germany

<sup>2</sup>Federal Maritime and Hydrographic Agency (BSH), Hamburg, Germany

*Correspondence to:* A. Seyler (aseyler@iup.physik.uni-bremen.de)

### Abstract

10 A three-year time series of ground-based MAX-DOAS measurements of NO<sub>2</sub> and SO<sub>2</sub> on the island Neuwerk has been analyzed for contributions from shipping emissions. The island is located in the German Bight, close to the main shipping lane into the river Elbe towards the harbor of Hamburg. Measurements of individual ship plumes as well as of background pollution are possible from this location, which is a few kilometers from the shipping lane. A simple approach using the column amounts of the oxygen molecule dimer or collision complex, O<sub>4</sub>, for the determination of the horizontal light path length has been  
15 applied to retrieve path-averaged volume mixing ratios. An excellent agreement between mixing ratios retrieved from NO<sub>2</sub> retrievals in the UV and visible parts of the spectrum has been found, showing the validity of the approach. Obtained mixing ratios of NO<sub>2</sub> and SO<sub>2</sub> are compared to co-located in-situ measurements showing good correlation on average with good agreement for well-mixed background pollution but systematic underestimation of plume concentrations by the MAX-DOAS O<sub>4</sub> approach. Comparing data before and after the introduction of stricter fuel sulfur content limits (from 1 % to 0.1 %) on 1 January 2015 in the North Sea emission control area (ECA), a significant reduction in SO<sub>2</sub> levels has  
20 been observed. For situations with wind from the open North Sea, where ships are the only local source of air pollution, the average mixing ratio of SO<sub>2</sub> decreased by a factor of eight, while for NO<sub>2</sub> in the whole time series from 2013 till 2016 no significant change in emissions has been observed. More than 2000 individual ship emission plumes have been identified in the data and analyzed for the emission ratio of SO<sub>2</sub> to NO<sub>2</sub>, yielding an average ratio of 0.3 for the years 2013/2014, decreasing significantly presumably due to lower fuel sulfur content in 2015/2016. By sorting measurements according to the prevailing wind direction and selecting two angular reference sectors representative for wind from open North Sea and coast excluding data with mixed air mass origin, relative contributions of ships and land-based sources to air pollution levels in the German Bight have been estimated to be  
25 around 40 % : 60 % for NO<sub>2</sub> as well as SO<sub>2</sub> in 2013/2014, dropping to 14 % : 86 % for SO<sub>2</sub> in 2015/2016.  
30  
35



## 1 Introduction

### 1.1 Shipping – a fast growing sector

Shipping has always been an important mode of transportation throughout the course of history. In contrast to the past, nowadays ships are almost exclusively carrying freight with the exception of a  
40 small number of cruise ships and ferries. Globalization of markets has lead to an enormous increase in world trade and consequently shipping traffic in the last decades, with growth rates being typically about twice that of the world gross domestic product (GDP) (Bollmann et al., 2010).

Shipping is generally the most energy efficient transportation mode, having the lowest greenhouse gas emissions per tonne per kilometer (3–60 gCO<sub>2</sub>/t/km), followed by rail (10–120 gCO<sub>2</sub>/t/km), road  
45 (80–180 gCO<sub>2</sub>/t/km) and air transport (435–1800 gCO<sub>2</sub>/t/km), which is by far the least efficient (Bollmann et al., 2010; IEA/OECD, 2009). At the same time, with a volume of 9.84 billion tons in 2014 it accounts for four fifths of the worldwide total merchandise trade volume (UNCTAD, 2015), as compared to for example the total air cargo transport volume of 51.3 million tons in 2014 (International Air Transport Association (IATA), 2015). As a result, shipping accounts for a significant part of the  
50 emissions from the transportation sector (Eyring et al., 2005a).

Despite growth rates now being lower compared to those prior to the 2008 economic crisis, seaborne trade is growing faster than the rest of the transportation sector, with an annual growth rate of 3–4 % in the years 2010 to 2014, compared to 2.0–2.6 % for the global merchandise volume (UNCTAD, 2014, 2015). The number of ships > 100 gross tonnage increased from around 31 000 in 1950 to 52 000 in  
55 1970 to 89 000 in 2001 (Eyring et al., 2005b) and is estimated to increase to about 150 000 in 2050 (Eyring et al., 2005a). At the same time, fuel consumption and emissions increased as well (Corbett and Koehler, 2003; Eyring et al., 2005a,b; Eyring et al., 2010b). Eyring et al. (2005a) predicted that future development of shipping emissions will depend more on the usage of new technologies and imposed regulations than on the economic growth rates.

### 60 1.2 Ship emission chemistry

The most important pollutants emitted by ships are carbon dioxide (CO<sub>2</sub>), carbon monoxide (CO), nitrogen oxides (NO<sub>x</sub> = NO + NO<sub>2</sub>), sulfur dioxide (SO<sub>2</sub>), black carbon (BC), volatile organic compounds (VOC) and particulate matter (PM) (Eyring et al., 2010a). This study focuses on NO<sub>2</sub> and  
65 SO<sub>2</sub>, because both are emitted in considerable amounts and both absorb light in the uv-visible spectral range and therefore can readily be measured by Differential Optical Absorption Spectroscopy (DOAS), which is explained in Sect. 3.1. In 2001, shipping emissions accounted for 15 % of all anthropogenic NO<sub>x</sub> and provided 8 % of all anthropogenic SO<sub>2</sub> emissions (ibid.).

NO<sub>x</sub> is predominantly formed thermally from atmospheric nitrogen and oxygen during high temperature combustion processes in ship engines in an endothermic chain reaction called the Zeldovich  
70 mechanism. The emitted NO<sub>x</sub> comprises mainly NO, with less than 25 % of NO<sub>x</sub> being emitted as NO<sub>2</sub> (Alföldy et al., 2013). Zhang et al. (2016) measured emission factors for gaseous and particulate pollutants on-board three Chinese vessels and found that more than 80 % of the NO<sub>x</sub> was emitted as NO and that emission factors were significantly different during different operation modes.

In the ambient atmosphere, NO is rapidly converted to NO<sub>2</sub> by reaction with ozone (O<sub>3</sub>) leading to  
75 a life time of only a few minutes. During daytime NO<sub>2</sub> is photolyzed by UV radiation ( $\lambda < 420$  nm) releasing NO and ground state oxygen radicals (O(<sup>3</sup>P)). In a three-body-collision reaction involving N<sub>2</sub> or O<sub>2</sub> the oxygen radical reacts with an oxygen molecule to reform ozone (Singh, 1987). When daylight is available, these reactions form a "null-cycle" and transformation between NO and NO<sub>2</sub> is very fast, leading to a dynamic equilibrium. This is also known as the Leighton photostationary state.



- 80 Deviations from the Leighton photostationary state occur in air masses, if the rates of the reactions of free radicals such as hydroperoxyl, HO<sub>2</sub>, or organic peroxy radicals, RO<sub>2</sub>, or Halogen oxides XO, where X=Cl, Br or I, compete with the reaction of NO with O<sub>3</sub>. The NO<sub>2</sub> formed in the reactions of HO<sub>2</sub> or RO<sub>2</sub> with NO is photolyzed and the O atoms reacts in the termolecular reaction with oxygen molecules O<sub>2</sub> to form O<sub>3</sub>. In tropospheric air-masses, typically, the X atoms released by the reaction of
- 85 NO with XO typically reacts rapidly with O<sub>3</sub> to reform XO. This changes the reaction of NO<sub>2</sub> to NO but does not produce O<sub>3</sub>. During night due to lack of photolysis, NO reacts rapidly with O<sub>3</sub> to form NO<sub>2</sub>. In addition NO<sub>3</sub>, the nitrate radical, is formed by reaction of NO<sub>2</sub> with O<sub>3</sub>. An equilibrium of NO<sub>2</sub> with NO<sub>3</sub> forming N<sub>2</sub>O<sub>5</sub>, the acid anhydride of nitric acid HNO<sub>3</sub>, results (Seinfeld and Pandis, 2006; Wayne, 2006).
- 90 During the day OH reacts with NO<sub>2</sub> in a three body reaction to form HNO<sub>3</sub>. An important sink for NO<sub>2</sub> in the troposphere is wet deposition of the resulting HNO<sub>3</sub>. The mean tropospheric lifetime of NO<sub>x</sub> varies between a few hours in summer and a few days in winter (Singh, 1987), depending on altitude. Inside ship plumes, Chen et al. (2005) found a substantially reduced lifetime of NO<sub>x</sub> of about 1.8 h compared to approximately 6.5 h in the background marine boundary layer (around noon). This
- 95 is attributed to enhanced levels of OH radicals in the plume.

Unlike for NO<sub>x</sub>, ship emissions of SO<sub>2</sub> are directly linked to the fuel sulfur content. Around 86 % of the fuel sulfur content is emitted as SO<sub>2</sub> (Balzani Lööv et al., 2014). Alföldy et al. (2013) found a linear relationship between SO<sub>2</sub> and sulfate particle emission and that only around 4.8 % of the total sulfur content is either directly emitted as or immediately transformed into particles after the emission. An

100 important sink for SO<sub>2</sub> is wet deposition after oxidation by OH radicals to the extremely hygroscopic sulfur trioxide (SO<sub>3</sub>) reacting rapidly with liquid water to form sulfuric acid (H<sub>2</sub>SO<sub>4</sub>) (Brasseur, 1999). Another important sink is dry deposition, leading to a lifetime of approximately one day in the boundary layer, which can be even shorter in the presence of clouds (Seinfeld and Pandis, 2006).

### 1.3 Influence on air quality and climate

- 105 Sulfate aerosols influence climate directly by scattering and absorption of solar radiation and indirectly by increasing cloud condensation, changing cloud reflectivity and lifetime (Eyring et al., 2010b; Lauer et al., 2007; Lawrence and Crutzen, 1999). In the presence of volatile organic compounds (VOC), nitrogen oxides are important precursors for the formation of tropospheric ozone and therefore photochemical smog. The release of both NO<sub>2</sub> and SO<sub>2</sub> leads to an increase in acidification of 3–10 %
- 110 in coastal regions contributing significantly to acid rain formation damaging eco-systems (Endresen et al., 2003; Jonson et al., 2000). The deposition of reactive nitrogen compounds causes eutrophication of ecosystem and decreases biodiversity (Galloway et al., 2003).

Around 70 % of shipping emissions occur within 400 km of land (Corbett et al., 1999), contributing substantially to air pollution in coastal areas (Eyring et al., 2010b). Ship emissions were found to

115 provide a dominant source of air pollution in harbor cities (Eyring et al., 2010a). In addition to that, transport of tropospheric ozone and aerosol precursors over several hundreds of kilometers also affect air quality, human health and vegetation further inland, far away from their emission point (Corbett et al., 2007; Eyring et al., 2010a; Eyring et al., 2010b).

NO<sub>2</sub> and SO<sub>2</sub> can cause a variety of respiratory problems. Tropospheric ozone is harmful to animals

120 and plants, causing various health problems. The EU legislation for O<sub>3</sub> exposure to humans has set a target limit of 120 µg/m<sup>3</sup> (~ 60 ppbv) for an maximum daily 8 hour mean but allows exceedences on 25 days averaged over 3 years (EU, 2008, 2016). As mentioned above, both NO<sub>2</sub> and SO<sub>2</sub> play a role in the formation of particles. Fine particles are associated with various health impacts like lung cancer, heart attacks, asthma and allergies (Corbett et al., 2007; Pandya et al., 2002; WHO, 2006).



#### 125 1.4 Attempts to decrease shipping emissions by stricter regulations

International ship traffic is subject to regulations of the International Maritime Organization (IMO). Shipping emissions are regulated by the International Convention for the Prevention of Pollution from Ships (MARPOL 73/78) Annex VI (DNV, 2008). This Annex was added in 1997 and entered into force in 2005. A revision with more stringent emission limits was adopted in 2008 and went into  
130 force 2010. With this, limits on sulfur content in heavy fuel oils globally are set and local Sulfur Emission Control Areas (SECA), later revised to general Emission Control Areas (ECA), along the North American coast and in the Baltic and North Sea (including the English Channel) are established with more stringent restrictions and controls. MARPOL introduced a global fuel sulfur limit of 4.5 %, which was reduced to 3.5 % in 2012 and will be further reduced in 2020 (or 2025 depending on a review  
135 in 2018) to 0.5 %. In the established ECAs, from 2010 on the limit was set to 1.5 % and was further reduced in 2010 to 1.0 %. Carrying out airborne in-situ measurements in several flight campaigns in the English Channel, North and Baltic Sea, Beecken et al. (2014) measured a 85 % compliance in 2011 and 2012 with the 1 % fuel sulfur limit. In the Gulf of Finland and Neva Bay area, Beecken et al. (2015) found a 90 % compliance in 2011 and 97 % compliance in 2012 with the 1 % fuel sulfur limit  
140 from ground-based, ship-based and helicopter-based in-situ measurements.

Recently, from 1 January 2015 on, the allowed fuel sulfur content in SECAs was further reduced to 0.1 %. Using in-situ measurements in Wedel at the bank of the river Elbe, a few kilometers downstream from Hamburg, Germany, Kattner et al. (2015) showed that in late 2014 more than 99 % of the measured ships complied with the 1 % sulfur limit and in early 2015 95.4 % of the measured ships  
145 complied with the new 0.1 % sulfur limit. By analyzing one and a half years of SO<sub>2</sub> measurements at the English Channel, Yang et al. (2016) found a three-fold reduction in SO<sub>2</sub> from 2014 to 2015. They estimated the lifetime of SO<sub>2</sub> in the marine boundary layer to be around half a day. Lack et al. (2011) measured a substantial drop of SO<sub>2</sub> emissions by 91 % when the investigated container ships entered the Californian ECA and switched from heavy fuel oil (HFO) with 3.15 % fuel sulfur content  
150 to marine gas oil (MGO) with 0.07 % fuel sulfur content. These estimates were obtained performing airborne in-situ measurements.

MARPOL Annex VI also establishes limits dependent on engine power for the emission of NO<sub>x</sub> from engines built after 2000 (Tier I), 2011 (Tier II) and 2016 (Tier III), but due to the slow penetration to the full shipping fleet, the impact on NO<sub>x</sub> emissions is not yet clear. Since 2010, a NO<sub>x</sub> emission  
155 control area exists around the North American coast and in the Caribbean, while for North and Baltic Sea the establishment of such a NECA is planned and was recently agreed on, but the future enforcement date is still unclear. The European Union also established a sulfur content limit of 0.1 % for inland waterway vessels and ships at berth in Community ports, which is in force since 1 January 2010 (EU, 2005).

The impact of shipping emissions on the North Sea for different regulation scenarios was investigated in a model study by the Helmholtz-Zentrum Geesthacht (HZG) within the scope of the Clean North Sea Shipping project. For current emissions a relative contribution of shipping emissions to air pollution in coastal regions of up to 25 % in summer and 15 % in winter for NO<sub>2</sub> and 30 % in summer and 12 % in winter for SO<sub>2</sub> was found (Aulinger et al., 2016). For the year 2030, the contribution of the  
165 continuously growing shipping sector to the NO<sub>2</sub> concentrations is predicted to decrease. The extent of reduction depends on the date on which the stricter Tier III regulations enter into force and on the fraction of the fleet complying to these regulations (i. e. the age of the fleet), with up to 80 % reduction if all ships comply (in the improbable case of a new ships only fleet). For SO<sub>2</sub>, the established fuel sulfur content limit of 0.1 % (ECA) and 0.5 % (globally) will lead to significant reductions, a further  
170 decrease is expected if the fraction of LNG powered ships grows (Matthias et al., 2016).



## 1.5 DOAS measurements of shipping emissions – previous studies

Optical remote sensing using the Differential Optical Absorption Spectroscopy (DOAS) technique to measure shipping emissions has been conducted before. For example Berg et al. (2012) performed airborne (from airplane and helicopter) DOAS measurements of NO<sub>2</sub> and SO<sub>2</sub> in ship plumes by measuring sea scattered light. Masieri et al. (2009) and Premuda et al. (2011) measured flow rate emissions (mass per second) of NO<sub>2</sub> and SO<sub>2</sub> for single ships with ground based MAX-DOAS measurements across the Giudecca Channel in the Venice lagoon. McLaren et al. (2012) measured nocturnal NO<sub>2</sub>/SO<sub>2</sub> ratios in ship plumes in the Strait of Georgia with the active long path DOAS technique. Balzani Lööv et al. (2014) tested and compared optical remote sensing methods (DOAS, LIDAR, UV camera) and in-situ (sniffer) methods for the measurement of shipping emissions in the framework of the SIRENAS-R campaign in the harbour of Rotterdam in 2009. Prata (2014) showed that a UV (SO<sub>2</sub>) imaging camera can be used to measure SO<sub>2</sub> in ship plumes at the Kongsfjord at Ny Ålesund, Svalbard and the harbor of Rotterdam.

The global pathways of the ships can be seen in long time averaged NO<sub>2</sub> measurements from various satellite instruments: from GOME over the Indian Ocean (Beirle et al., 2004), from SCIAMACHY on board ENVISAT over the Indian Ocean and the Red Sea (Richter et al., 2004), in even more detail with a lot more visible ship tracks from GOME-2 on board MetOp-A (Richter et al., 2011). The higher resolution of OMI yielded ship tracks in the Baltic Sea (Ialongo et al., 2014) and in all European seas (Vinken et al., 2014).

## 1.6 The MeSMarT project

The current study is part of the project MeSMarT (Measurements of Shipping emissions in the Marine Troposphere), which is a cooperation between the University of Bremen (Institute of Environmental Physics, IUP) and the Federal Maritime and Hydrographic Agency (Bundesamt für Seeschifffahrt und Hydrographie, BSH), supported by the Helmholtz Zentrum Geesthacht (HZG). It aims to monitor background concentration as well as elevated signals of gases and particles related to ship emissions with various methods to cover a wide range of relevant pollutants and their spatial and seasonal distribution to estimate the influence of ship emissions on the chemistry of the atmospheric boundary layer (<http://www.mesmart.de/>).

## 1.7 Aims of this study

The objectives of this study are to assess whether measurements of individual ship plumes are feasible with a ground-based MAX-DOAS instrument, to compare MAX-DOAS with co-located in-situ measurements, to estimate the contribution of ships and land-based sources to air pollution in a North Sea coastal region, to survey the effect of fuel sulfur content regulations on SO<sub>2</sub> concentrations in the marine boundary layer and to analyze the SO<sub>2</sub> to NO<sub>2</sub> ratio in plumes to gain information about plume chemistry and the sulfur content in shipping fuels.

In the following, first the measurement site is described, wind statistics and data availability is shown. After this, the Differential Optical Absorption Spectroscopy (DOAS), the MAX-DOAS instrumentation and measurement geometry as well as the DOAS data analysis approach used are briefly described. In the next section, selected results from this study are presented: for example the measured differential slant column densities (DSCD), the retrieved path-averaged volume mixing ratios, the comparison to in-situ measurements, the diurnal and weekly variability, the contribution estimates for ships as well as land-based sources and the analysis of SO<sub>2</sub> to NO<sub>2</sub> ratios in ship plumes. Finally, a summary is given and conclusions are drawn.



## 2 Measurement site

215 The measurements presented within this study were taken on the North Sea island Neuwerk. This is a small island with the size of about 3 km<sup>2</sup> and 33 inhabitants in the German Wadden Sea in the German Bight. It is located northwest of Cuxhaven at the mouth of the river Elbe, roughly 8–9 km off the Coast, as can be seen from the map in Fig. 1 A).

The North Sea has one of the highest ship densities in the world (Matthias et al., 2016). The majority of ships that arrive in the port of Hamburg sail through the German Bight and the river Elbe and therefore pass the island Neuwerk, where our measurement site is located. Hamburg is among the largest ports worldwide, together with Rotterdam and Antwerp one of the three largest ports in Europe, having a 4–5 % increase in container volume in the last years (UNCTAD, 2014, 2015). Hamburg also experiences a large increase in the number of cruise ships, having 176 ship calls in 2014 compared to 25 in the year 2005 (Statistische Ämter des Bundes und der Länder (Statistikamt Nord), 2015).

Neuwerk is relatively close to the main shipping lane from the North Sea into the river Elbe. On this highly frequented waterway, nearly all ships to and from the port of Hamburg and the Kiel canal (connection to the Baltic Sea) pass the island at a distance of 6–7 km, as shown in Fig. 1 B). Still close, but further away to the west are the shipping lanes to the Weser river to the ports of Bremerhaven and Bremen and to Wilhelmshaven (JadeWeserPort).

Neuwerk is surrounded by the Hamburg Wadden Sea National Park and there are no significant sources of air pollution on the island itself, making it a very suitable station for measurements of shipping emissions.

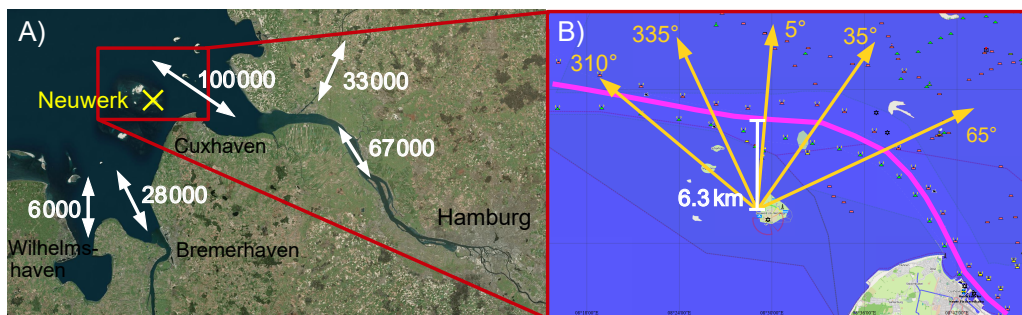


Figure 1: **A)** Location of the measurement site Neuwerk in the German Bight, close to the mouth of the river Elbe. Number of ship movements (data from 2011/2012) is given by the white numbers. Data source: German Federal Waterways and Shipping Administration (WSV, 2013, 2014) Map source: <http://www.bing.com/maps/> (01.04.2014)

**B)** Azimuthal viewing directions of the MAX-DOAS instrument towards the main shipping lane (highlighted by the magenta line), passing the island in the north in a distance of 6–7 km. Map source: <http://www.freie-tonne.de> (16.07.2013)

235 The ship emission measurements presented in this study were carried out with a MAX-DOAS instrument (see Sect. 3.2) which measures in multiple azimuthal viewing directions, as shown in Fig. 1 B), pointing directly towards the shipping lane while the different viewing azimuth angles cover a large part of the region.

Several measurement devices, including the two-channel MAX-DOAS instrument (for UV and visible spectral range), an Airpointer in-situ measurement device (measuring CO<sub>2</sub>, NO<sub>x</sub>, SO<sub>2</sub> and O<sub>3</sub>), a high volume filter sampler and passive samplers as well as a weather station and an AIS (Automatic



Identification System) signal receiver, are positioned on the main platform of a radar tower at a height of about 30 m (see Fig. 2).



Figure 2: Radar tower Neuwerk with MAX-DOAS and in-situ measurement device

Additional wind data is available from measurements by the Hamburg Port Authority (HPA) on  
245 Neuwerk and the neighboring island Scharhörn. The seasonal distribution of wind directions on  
Neuwerk is shown in Fig. 3.

In spring and summer, on a high percentage of days the wind blows from the open North Sea, where  
shipping emissions are the only significant source of local air pollution. Consequently, the site for the  
measurements provides an optimal opportunity for measurements of ship emission plumes. In winter,  
250 southerly directions prevail, bringing potentially polluted air masses from the land and blowing the  
ship emission plumes away from the measurement site. In addition, as the MAX-DOAS technique  
requires daylight and because of the short days and the low sun resulting in less UV light reaching the  
surface, measurements are in general sparse in winter months, especially for SO<sub>2</sub>, which has its strong  
absorption features in the UVB. This effect can be seen in winter gaps in Fig. 4, which presents the  
255 data availability for more than two years of measurements on Neuwerk.

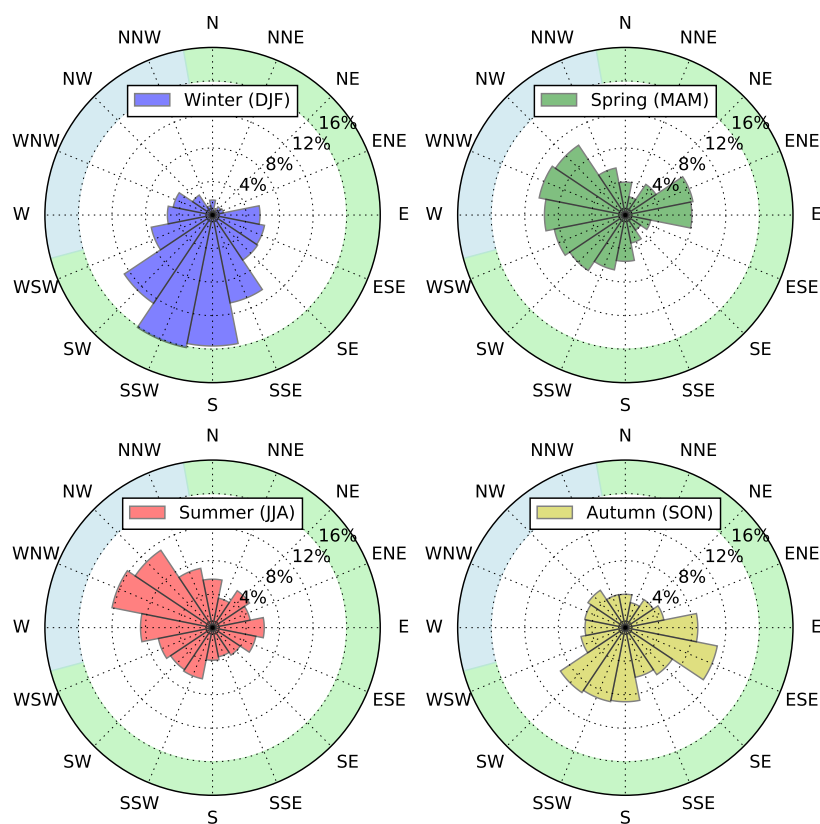


Figure 3: Seasonal wind direction distribution for Neuwerk (Data from 04.07.2013 to 26.10.2015). The colored sectors show directions with wind from the coast (green) and from the open North Sea (blue).

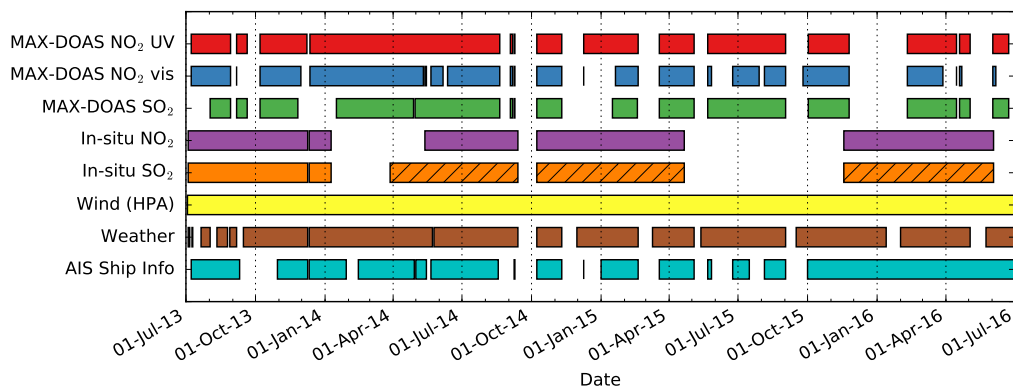


Figure 4: Data availability in the analyzed measurement period between July 2013 and July 2016. From March 2014 on (hatched), there were instrumental problems with the in-situ  $\text{SO}_2$  instrument resulting in a strong oscillation of  $\pm 0.5$  ppb superimposing the data. However, this data can still be used for the comparison of long-term averages.

### 3 Measurement techniques, instruments and data analysis

#### 3.1 Differential Optical Absorption Spectroscopy (DOAS)

The principle of optical absorption spectroscopy is the attenuation of light intensity while passing through an absorbing medium, described by the well-known Lambert-Beer-law (also known as Beer-Lambert-Bouguer law). For the general case of electromagnetic radiation passing through an anisotropic medium having a number density  $n$  and a temperature and pressure dependent absorption cross section  $\sigma$  of an absorbing species along the light path  $s$ , the measured intensity at wavelength  $\lambda$  is given by

$$I(s, \lambda) = I_0(\lambda) \cdot \exp \left\{ - \int_0^s n(s') \cdot \sigma(\lambda, T(s'), p(s')) \cdot ds' \right\} \quad (1)$$

where the intensity of radiation entering the medium is  $I_0$ . For measurements in the atmosphere, this simple model has to be extended by considering multiple trace gases having different absorption cross sections and light scattering on air molecules (Rayleigh scattering), aerosol particles or water droplets (Mie scattering) as well as inelastic scattering by air and trace gas molecules (Raman scattering). The latter is responsible for the Ring effect (Grainger and Ring, 1962), another important extinction process, which can be described by a pseudo cross-section.

The key and original idea of the Differential Optical Absorption Spectroscopy (DOAS) is to separate the optical depth and the absorption cross-sections  $\sigma_i(\lambda)$  into a slowly varying function  $\sigma_{i,0}(\lambda)$  accounting for elastic scattering and broadband absorption structures and described by a low-order polynomial and a rapidly varying part  $\sigma'_i(\lambda)$ , the differential cross-section, considering the narrow-band absorption structures (Platt and Perner, 1980; Platt and Stutz, 2008). The absorption cross-sections are measured in the laboratory. Polynomial and differential cross sections are fitted to the measured optical thickness  $\ln(I/I_0)$  in the linearized so-called DOAS equation to retrieve the slant column density of a trace gas as the integrated number density along the light path  $\text{SCD}_i = \int n_i(s) ds$ :

$$\ln \left( \frac{I(\lambda)}{I_0(\lambda)} \right) = - \sum_{i=1}^N \text{SCD}_i \cdot \sigma'_i(\lambda) - \sum_p c_p \cdot \lambda^p + \text{RESIDUAL}(\lambda) \quad (2)$$



### 3.2 MAX-DOAS instrument and viewing geometry

The Multi-AXis DOAS (MAX-DOAS) technique (Hönninger et al., 2004; Wittrock et al., 2004) is a passive remote sensing method measuring scattered sunlight. The MAX-DOAS instrument used in this study, comprises of a telescope mounted on a pan-tilt head, an optical fiber bundle, two spectrometers for UV and visible spectral range respectively, equipped with two CCD (charge coupled device) 2D array detectors operated by a computer. The telescope which is attached to the outer sheathing of the circular platform of the Neuwerk radar tower is used to collect the light from a specific viewing direction and to inject the light into the optical fiber. The combination of converging lens and light fiber leads to an opening angle of about  $1.1^\circ$ . The pan-tilt head allows the instrument to point in different azimuth angles (panning) as well as different elevation angles (tilting). Dark measurements, which are needed for the determination of the CCD's dark signal are undertaken on a daily basis. Also on a daily basis line lamp measurements are taken using an internally mounted HgCd lamp for the wavelength calibration of the spectra and the determination of the slit function of the instrument. The spectral resolution, represented by the FWHM of the slit function of the instrument, is about 0.4 nm for the UV and 0.7 nm for the visible channel.

The optical light fiber cable is a bundle of cylindrical, thin and flexible quartz fibers, guiding the light from the telescope to the two temperature-stabilized spectrometers with attached CCD detectors inside the weatherproof platform building. The UV and visible instrument consist of identical Andor Shamrock SR-303i imaging spectrographs, a grating spectrometer in "Czerny-Turner" design with a focal length of 303 mm. The gratings in use are different, the UV instrument is equipped with a 1200 grooves/mm, 300 nm blaze angle grating and the visible instrument with a 600 grooves/mm, 500 nm blaze angle grating. For the UV, a Princeton NTE/CCD 1340/400-EMB detector with a resolution of  $1340 \times 400$  pixels and a pixel size of  $20 \times 20$  microns, cooled to  $-35^\circ\text{C}$ , is used. For the visible spectral range, an Andor iDus DV420-BU back-illuminated CCD detector with a resolution of  $1024 \times 255$  pixels and a pixel size of  $26 \times 26$  microns, cooled as well to  $-35^\circ\text{C}$ , is used.

The measurement geometry for the ground-based MAX-DOAS measurements on Neuwerk is sketched in Fig. 5. To measure ship emissions, the telescope is pointed towards the horizon, measuring right through the emitted ship plumes. A close-in-time zenith sky measurement is used as a reference so that the retrieved tropospheric differential slant column density (DSCD) is the difference of the slant column densities (SCD) along the two paths:  $\text{DSCD} = \text{SCD}_1 - \text{SCD}_2$ . The stratospheric light path and trace gas absorption is approximately the same for both measurements and therefore cancels out which is important for  $\text{NO}_2$  which is also present in the stratosphere. This approach also minimizes possible instrumental artifacts.

The assumption that the vertical part of the light path cancels out when taking the difference between off-axis and zenith sky (reference) measurement off course is only valid if the  $\text{NO}_2$  in the air above the instrument, which is of no interest to us here, is spatially homogeneously distributed. This is usually the case for stratospheric  $\text{NO}_2$ . If a spatially limited pollution plume from ships, power plants etc. is blown above the radar tower, the mentioned assumption is violated, leading to errors in the derived qualities.

If there is no plume in the horizontal light path, but in the air above the radar tower, the retrieved DSCD would be negative. This happens if urban pollution plumes from land pass over the site. Should significant amounts of the radiation reaching the instrument pass through clouds then as a result of the multiple scattering in the cloud the interpretation of the measured DSCD is more challenging.

**Remark concerning the elevation angles of our instrument:** The value in the following text is referred to as  $0^\circ$  elevation angle is in reality an elevation angle of  $0.6^\circ$ . The acceptance angle of our telescope is about  $1.1^\circ$  and it has a circular field of view. This means that the field of view extends vertically from  $0.05^\circ$  to  $1.05^\circ$  (nearly  $0^\circ$  to  $1^\circ$ ). Thus the  $0^\circ$  line-of-sight represents an average over this field of view. This has the advantage that the surface, which may have spectral structures, is not

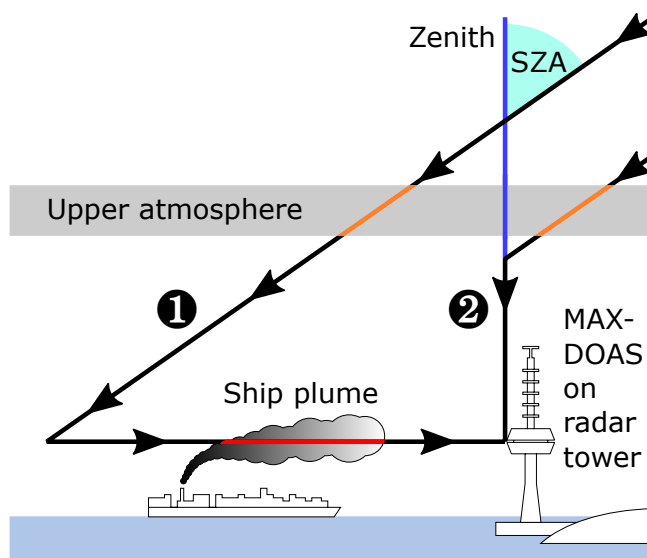


Figure 5: Measurement geometry for MAX-DOAS measurements on Neuwerk with schematic light paths for off-axis (1) and zenith sky reference measurements (2) for an exemplary solar zenith angle (SZA) of  $55^\circ$

explicitly probed. The same averaging over the relevant solid angle occurs for the higher elevation angles like 2, 4, 30 and  $90^\circ$ .

### 3.3 DOAS data analysis and fit settings

The recorded spectra are spectrally calibrated using a daily acquired HgCd line lamp spectrum and the dark signal of the CCD detector is corrected using daily nighttime dark measurements. The logarithm of the ratio of measured off-axis (viewing towards the horizon) spectrum and reference (zenith sky) spectrum gives the optical thickness (also called optical depth) for the DOAS equation (2). Multiple trace gas absorption cross sections obtained from laboratory measurements, as well as a low-order polynomial, are then fitted simultaneously to the optical depth. The retrieved fit parameters are the slant column densities of the various absorbers and the coefficients of the polynomial. The fits were performed with the software NLIN\_D (Richter, 1997).

The settings and fitted absorbers vary according to the spectral range used. For the retrieval of  $\text{NO}_2$  in the UV, a fitting window of 338–370 nm was used and for  $\text{NO}_2$  in the visible a fitting window of 425–497 nm, both adapted from experiences during the CINDI (Roscoe et al., 2010) and MAD-CAT ([http://joseba.mpch-mainz.mpg.de/mad\\_cat.htm](http://joseba.mpch-mainz.mpg.de/mad_cat.htm)) inter-comparison campaigns. The oxygen-collision complex  $\text{O}_2\text{-O}_2$ , often denoted as  $\text{O}_4$ , is simultaneously retrieved from both  $\text{NO}_2$  fits. The fit parameters for the DOAS fit of  $\text{NO}_2$  and  $\text{SO}_2$  are summarized in detail in Table 1.

For the retrieval of  $\text{SO}_2$ , several different fitting windows between 303 and 325 nm have been used in previous ground-based studies (Bobrowski and Platt, 2007; Galle et al., 2010; Irie et al., 2011; Lee et al., 2008; Wang et al., 2014). This results from the need to find a compromise between the strong ozone absorption around 300 nm on the one hand and the rapid decrease of the differential absorption of  $\text{SO}_2$  at higher wavelengths on the other hand, limiting the choice of the fitting window. In this study, a fitting window of 307.5–317.5 nm was found as the optimal range for our instrument, which



350 is similar to recommendations in Wang et al. (2014). The fit parameters for the DOAS fit of SO<sub>2</sub> are summarized in detail in Table 2.

Only SO<sub>2</sub> measurements with a RMS lower than  $2.5 \times 10^{-3}$  have been taken into account for the statistics, filtering out bad fits with ozone interferences in low light and bad weather conditions.

Table 1: DOAS fit settings for the retrieval of NO<sub>2</sub> and O<sub>4</sub> in UV and visible spectral range

Parameter	NO <sub>2</sub> (UV)	NO <sub>2</sub> (visible)
Fitting window	338–370 nm	425–497 nm
No. of poly. coeff.	5 (polynomial degree 4)	4 (polynomial degree 3)
Intensity offset	Constant	Constant
Zenith reference	Coinciding zenith measurement <sup>1</sup>	Coinciding zenith measurement <sup>1</sup>
SZA range	Up to 85° SZA	Up to 85° SZA
O <sub>3</sub>	223 K & 243 K (Serdyuchenko et al., 2014)	223 K (Serdyuchenko et al., 2014)
NO <sub>2</sub>	298 K (Vandaele et al., 1996)	298 K (Vandaele et al., 1996)
O <sub>4</sub>	293 K (Thalman and Volkamer, 2013)	293 K (Thalman and Volkamer, 2013)
H <sub>2</sub> O	–	293 K (Lampel et al., 2015)
HCHO	297 K (Meller and Moortgat, 2000)	–
Ring	SCIATRAN (Rozanov et al., 2014)	SCIATRAN (Rozanov et al., 2014)

<sup>1</sup> Interpolation in time between the zenith measurements directly before and after the off-axis scan.

Table 2: DOAS fit settings for the retrieval of SO<sub>2</sub>

Parameter	SO <sub>2</sub> (UV)
Fitting window	307.5–317.5 nm
No. of poly. coeff.	4 (polynomial degree 3)
Intensity offset	Constant & slope
Zenith reference	Coinciding zenith measurement <sup>1</sup>
SZA range	Up to 75° SZA
O <sub>3</sub>	223 K & 243 K (Serdyuchenko et al., 2014)
NO <sub>2</sub>	298 K (Vandaele et al., 1996)
SO <sub>2</sub>	293 K (Bogumil et al., 2003)
Ring	SCIATRAN (Rozanov et al., 2014)

<sup>1</sup> Interpolation in time between the zenith measurements directly before and after the off-axis scan.

### 3.4 Conversion of slant column densities (SCD) to volume mixing ratios (VMR)

355 To compare DOAS measurements (trace gas columns) with, for example, in-situ measurements (concentrations), the retrieved slant column densities need to be converted to volume mixing ratios. The volume mixing ratio  $\text{VMR} = n_x/n_{\text{air}}$  of a gas  $x$  is defined as the ratio of the number densities of the gas and air and describes its atmospheric number fraction. The number density of air can be estimated using the ideal gas law:



$$n_{\text{air}} = \frac{N_{\text{air}}}{V_{\text{air}}} = \frac{p_{\text{air}} \cdot k_{\text{B}}}{T_{\text{air}}} = \frac{p_{\text{air}} \cdot N_{\text{A}}}{T_{\text{air}} \cdot R} \quad (3)$$

with the Boltzmann constant  $k_{\text{B}}$ , Avogadro constant  $N_{\text{A}}$  and universal gas constant  $R$ . The retrieval  
 360 of the number density of the trace gas from the DOAS measurements can be done in different ways:

One possibility is to use a geometric approximation with a simple geometric air mass factor  $\text{AMF}_{\text{geom}} = \frac{1}{\sin(\alpha)}$  for the elevation angle  $\alpha$  to first convert the slant columns to vertical columns. The tropospheric vertical column density (VCD) divided by a typical mixing layer height (MLH) in which the trace gas is assumed to be well-mixed then gives the number density of the trace gas:

$$n_{x,\text{geom}} = \frac{\text{VCD}_{\text{trop}}}{\text{MLH}} \quad \text{with} \quad \text{VCD}_{\text{trop}} = \frac{\text{SCD}_{\alpha} - \text{SCD}_{90^{\circ}}}{\sin(\alpha)^{-1} - \sin(90^{\circ})^{-1}} = \frac{\text{DSCD}_{\alpha}}{\sin(\alpha)^{-1} - 1} \quad (4)$$

365 A disadvantage of this method is the assumption of a typical mixing layer height, if no independent measurements of the MLH (e. g. using LIDAR) is available. Another disadvantage is that this approach does not account for changes in the light path due to changing weather (clouds, fog) and aerosol conditions. In addition, the profile will not be box-shaped in reality and the geometric AMF does only hold for large elevation angles.

370 A second possibility, which was applied for the measurements presented in this study, is to use the mountain MAX-DOAS-approach developed by Gomez et al. (2014). The basic principle of this method is the assumption that the signal for horizontal measurements (i. e. for an elevation angle of  $0^{\circ}$ ) is dominated by the horizontal part of the light path after the last scattering event. The length  $L$  of this horizontal part of the light path can then be estimated using the slant column density of the  
 375  $\text{O}_4$ -molecule which has a well-known number density in the atmosphere:

$$L_{\text{O}_4} = \frac{\text{SCD}_{\text{O}_4,\text{horiz}} - \text{SCD}_{\text{O}_4,\text{zenith}}}{n_{\text{O}_4}} = \frac{\text{DSCD}_{\text{O}_4}}{n_{\text{O}_4}} \quad (5)$$

Here,  $n_{\text{O}_4} = (n_{\text{O}_2})^2 = (0.20942 \cdot n_{\text{air}})^2$  can be easily calculated via Eq. (3) from the measured temperature and pressure.

Knowing the path length, it is then possible to calculate the average number density of our trace gas  $x$  along this horizontal path and the path-averaged volume mixing ratio:

$$n_{x,\text{O}_4} = \frac{\text{SCD}_{x,\text{horiz}} - \text{SCD}_{x,\text{zenith}}}{L_{\text{O}_4}} = \frac{\text{DSCD}_x}{L_{\text{O}_4}} \quad \text{and} \quad \text{VMR} = \frac{n_x}{n_{\text{air}}} \quad (6)$$

380 As using the  $\text{O}_4$  slant column density, this approach takes into account the actual light path and its variation with aerosol loading and also needs no assumption on the typical mixing layer height, therefore overcoming the disadvantages of the simple geometric approximation. Since the  $\text{O}_4$ -DSCD is retrieved simultaneously to  $\text{NO}_2$  in both the UV and visible DOAS fit for  $\text{NO}_2$ , this approach can be applied to  $\text{NO}_2$  retrieved in both fitting ranges. The approach can also be applied to  $\text{SO}_2$ , although  
 385 the difference of light paths due to the slightly different fitting windows in the UV for  $\text{O}_4$  ( $\text{NO}_2$ ) and  $\text{SO}_2$  introduces an uncertainty which has to be accounted for. In this study, a scaling factor of 0.8 was used, retrieved from extrapolation of the ratio of the  $\text{O}_4$  columns in the longer wavelength UV and visible measurements.



Using this approach, several problems can arise from the division by the differential slant column  
390 density of  $O_4$ . For example if the  $O_4$  DSCD is negative, which can happen at low signal-to-noise-ratio  
(SNR) DOAS fits (e. g. under bad weather conditions), the resulting path length will be negative. If at  
the same time the trace gas DSCD is positive, then the trace gas volume mixing ratio will be negative  
as well, a non-physical result. However, even when there is no  $NO_2$  or  $SO_2$ , there is still some noise  
and therefore the retrieved VMR are not exactly zero, but scatter around zero, so slightly negative  
395 values have to be included when averaging over time to avoid a high bias. If, on the other hand, the  
 $O_4$  DSCD is close to zero, the path length will be very small leading to extremely high (positive or  
negative) mixing ratios which are unrealistic.

To adress both problems, measurements with negative or small retrieved horizontal path lengths are  
filtered. For the measurements on Neuwerk, with respect to the characteristics of the measurement  
400 site, a minimum path length of 5 km seems to be a reasonable limit. This value provides the best  
compromise between the number of rejected bad measurements and the total number of remaining  
measurements for  $NO_2$  in UV and visible as well as for  $SO_2$ . For statistics on differential slant column  
densities on the other hand, no such filtering is applied since negative values are not unphysical in  
this case and just mean that there is more trace gas absorption in the reference than in the off-axis  
405 measurement.

The  $O_4$  scaling approach was previously applied to measurements from high mountain sites only, for  
example by Gomez et al. (2014) at the Izaña Atmospheric observatory on Tenerife (Canary Islands)  
or by Schreier et al. (2016) at Zugspitze (Germany) and Pico Espejo (Venezuela). The fact that our  
instrument is located on a radar tower in a height of about 30 m above totally flat surroundings (the  
410 German Wadden Sea) means that it is appropriate to apply this approach to our measurements on  
Neuwerk.

**Remark concerning the elevation angles of our instrument:** Since the opening angle or field  
of view of our instrument is about  $1.1^\circ$ , looking at  $0^\circ$  elevation towards the horizon would result in  
partially (with the lower half of our circular field of view) looking onto the ground (or sea surface,  
415 depending on tide). To avoid possible problems arising from this like spectral interferences, our  
instrument is looking slightly upward. What in this study is referred to as  $0^\circ$  elevation angle is in  
reality an elevation angle of around  $0.6^\circ$ . With our opening angle of about  $1.1^\circ$  and a circular field of  
view this means the field of view extends vertically from  $0.05^\circ$  to  $1.05^\circ$ , so  $0^\circ$  elevation means actually  
a field of view from nearly  $0^\circ$  to  $1^\circ$ . The same is true for the higher elevation angles like 2, 4, 30 and  
420  $90^\circ$ . Since deviations arising from this are small, this is neglected in the following.

### 3.5 In-situ instrumentation

In addition to the MAX-DOAS instrument, also in-situ observations are taken, using the Airpointer, a  
commercially available system which combines four different instruments in a compact, air-conditioned  
housing. The manufacturer is recordum (Austria), distributed by MLU ([http://mlu.eu/recordum-  
425 airpointer/](http://mlu.eu/recordum-airpointer/)). The Airpointer device measures carbon dioxide ( $CO_2$ ), nitrogen oxides ( $NO_x = NO + NO_2$ ), sulfur dioxide ( $SO_2$ ) and ozone ( $O_3$ ) using standard procedures. Table 3 shows more detailed  
information about the different included instruments, their measurement methods, precision, and time  
resolution.

In this study the in-situ 1-minute-means of all compounds were used.  $NO_2$  itself is not directly  
430 measured but calculated internally by subtracting the measured NO from the measured  $NO_x$  concen-  
tration.



Table 3: Airpointer in-situ device: measured trace gases, corresponding measuring techniques, measuring ranges and detection limits [Source: recordum/MLU (manufacturer), <http://mlu.eu/recordum-airpointer/>]

Trace gas	CO <sub>2</sub>	O <sub>3</sub>	NO, NO <sub>2</sub>	SO <sub>2</sub>
<b>Measuring technique</b>	Non-dispersive IR spectroscopy LI-COR LI820	UV absorption (EN 14625)	NO Chemi-luminescence (EN 14211)	UV fluorescence (EN 14212)
<b>Detection limit</b>	1 ppm	0.5 ppb	0.4 ppb	0.25 ppb
<b>Measuring range</b>	up to 20 000 ppm	up to 200 ppm	up to 20 ppm	up to 10 ppm
<b>Time resolution</b>	1 s	<30 s	<60 s	<90 s

## 4 Results

### 4.1 Measured slant column densities of NO<sub>2</sub> and SO<sub>2</sub>

In this study, three years of continuous MAX-DOAS measurements on Neuwerk have been evaluated.

435 Figure 6 shows for one example day in summer 2014 the measured differential slant column densities of NO<sub>2</sub> in UV and visible spectral range as well as of SO<sub>2</sub> for the 0° elevation angle (viewing to the horizon) and the -25° azimuth angle (approximately NNW direction, see Fig. 1). Sharp peaks in the curves originate from ship emission plumes passing the line of sight of the instrument. On this day, elevated levels of the pollutant NO<sub>2</sub> have been measured in the morning, corresponding to a  
 440 polluted air mass coming from land, which appears as an enhanced, slowly varying NO<sub>2</sub> background signal below the peaks. The systematic difference between the red curve (NO<sub>2</sub> in the UV) and the blue curve (NO<sub>2</sub> in the visible) emerges from the longer light-path in the visible due to more intense Rayleigh scattering in the UV (wavelength dependence  $\propto \lambda^{-4}$ ). This is further investigated in Sect. 4.3 below.

445 By comparing the black SO<sub>2</sub> curve with the red and blue NO<sub>2</sub> curves it can be seen that for many of the NO<sub>2</sub> peaks there is a corresponding and simultaneous SO<sub>2</sub> peak, but not for all of them. This illustrates that the sulfur content in the fuel of the measured ships varies. A more dirty fuel with higher sulfur content leads to higher SO<sub>2</sub> emissions (see also Sect. 1).

450 By comparing measurements in different azimuthal viewing directions, the movement direction of the ship (and its plume) can be easily distinguished. The zoom in on the right of Fig. 6 shows the visible NO<sub>2</sub> measurements in different azimuth directions for one example peak from the time series shown on the left. The color-coded viewing directions (see also Fig. 1) are sketched schematically below. From the measurements it can be seen that the emitted plume was consecutively measured in all directions at different points in time. It was first measured in the easternmost viewing directions  
 455 and at last in the westernmost direction, indicating that the ship and its plume moved from east to west.

For the identification of sources for air pollution on Neuwerk, the wind direction distribution for the differential slant column densities of NO<sub>2</sub> and SO<sub>2</sub> measured in 2013 and 2014 is plotted for four different elevation angles (0°, 2°, 4° and 30°) in Fig. 7. When the wind is coming from the open  
 460 North Sea (blue shaded sector) the measured NO<sub>2</sub> and SO<sub>2</sub> DSCD are clearly lower than for other directions, for which the wind is coming from the coast (green shaded sector) and blows land-based air pollution to the island. The wind direction dependence is more or less similar for both trace gases but with a higher fraction of ship related signals in the overall SO<sub>2</sub> columns. The values are especially

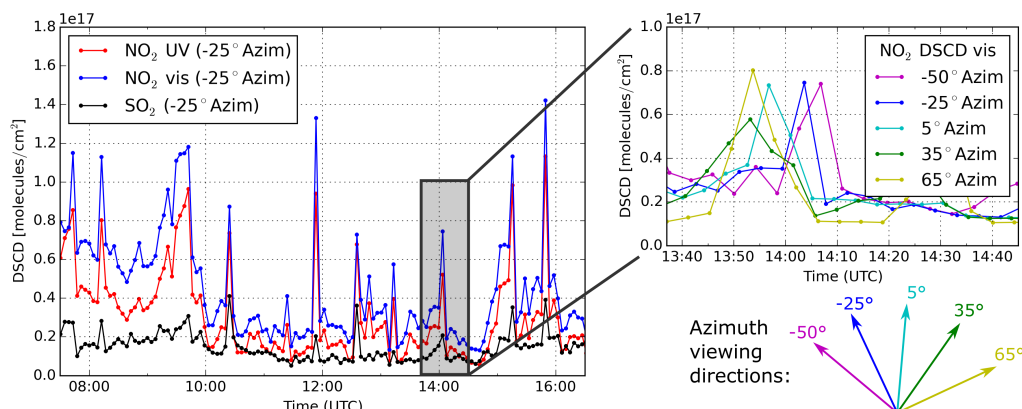


Figure 6: NO<sub>2</sub> (UV and visible) and SO<sub>2</sub> differential slant column densities measured in 0° elevation and the -25° viewing azimuth angle (approximately NNW direction) on Neuwerk on Wednesday, 23 July 2014. The excerpt on the right shows for one example peak the NO<sub>2</sub> (vis) measurements in different azimuth viewing directions, which are schematically sketched below.

high when the wind is coming from the cities of Cuxhaven (ESE direction) and Bremerhaven (SSE)  
 465 for both NO<sub>2</sub> and SO<sub>2</sub>.

Elevation angle sequences of slant columns (vertical scanning) contain information on the vertical  
 distribution of trace gases. For lower elevation angles, the measured trace gas slant columns for  
 tropospheric absorbers are usually higher, because of the longer light path in the boundary layer.  
 This can be seen in Fig. 7, showing highest NO<sub>2</sub> and SO<sub>2</sub> DSCD in the lowest elevation angle  
 470 (0°, blue bars), and decreasing values while scanning upwards. The relative proportions of the NO<sub>2</sub>  
 measurements (Figure 7 A) in 0° elevation compared to the measurements in 2° and 4° elevation is  
 clearly different for the various wind directions. For wind directions from WSW to N to ESE, the ratio  
 between the differential slant column densities in the lowest elevation angle to the higher elevations  
 is much larger than for the southerly wind directions, corresponding to more NO<sub>2</sub> in lower altitudes  
 475 in the north of the island. These directions with enhanced values coincide with the course of the  
 main shipping lane, which comes from the WSW direction (the English Channel, the Netherlands,  
 East Frisian Islands), passes the island in the north and runs close to the city of Cuxhaven (ESE  
 direction) into the river Elbe. This indicates that these enhanced columns measured in low altitudes  
 are coming from ships. For SO<sub>2</sub> (Figure 7 B), the fraction of measurements from the shipping lane  
 480 on the overall emissions is higher than for NO<sub>2</sub>, showing that in the German Bight shipping is a very  
 important source of SO<sub>2</sub> emissions, while for NO<sub>2</sub> land-based pollution sources (traffic, industry) are  
 more important. This will be further discussed in Sect. 4.8

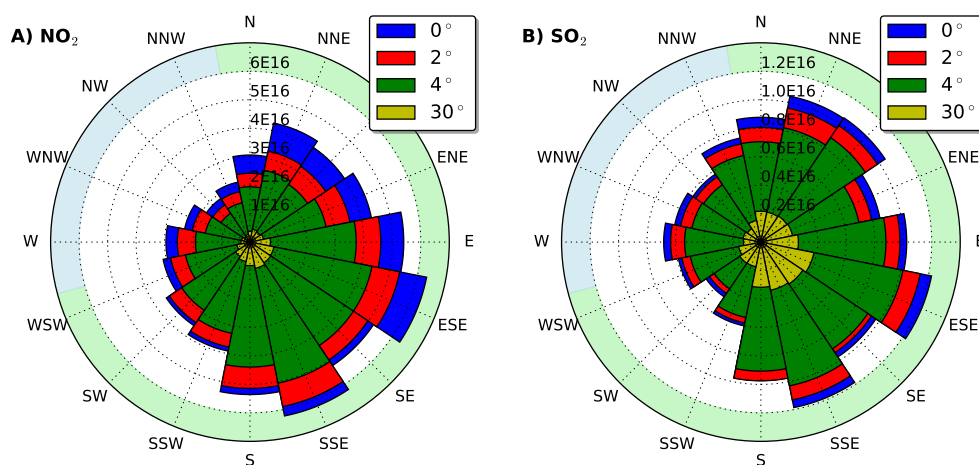


Figure 7: Wind direction distribution of the UV  $\text{NO}_2$  (A) and  $\text{SO}_2$  (B) differential slant column densities measured in the main viewing direction in  $0^\circ$ ,  $2^\circ$ ,  $4^\circ$  and  $30^\circ$  elevation in the years 2013 and 2014. The bars are plotted on top of each other, i. e. the highest values were measured in the lowest elevation angle (blue bars). The colored sectors show directions with wind from the coast (green) and open North Sea (blue).

#### 4.2 Retrieved volume mixing ratios of $\text{NO}_2$ and $\text{SO}_2$ by using $\text{O}_4$ as a tracer for the horizontal light path length

485 For the example day presented in Fig. 6 the path-averaged volume mixing ratios retrieved with the approach presented in Sect. 3.4 using  $\text{O}_4$  as a tracer for the light path length are shown in Fig. 8.

From the mathematics of the approach one would expect a good agreement between the  $\text{NO}_2$  volume mixing ratios retrieved in UV and visible if  $\text{NO}_2$  is well mixed in the boundary layer, since averaging constant values over different paths should give equal mean values. In the figure, in fact one can see a very good agreement between both  $\text{NO}_2$  volume mixing ratios, in particular for situations characterized by background pollution.

495 If  $\text{NO}_2$  is not distributed homogeneously along the light path, which is the case in the presence of individual ship exhaust plumes, one can expect different values for the means over the two light paths as they probe different parts of the  $\text{NO}_2$  field. Such differences can be identified in the figure by looking at the peaks.

The light path in the visible spectral range is longer than in the UV because of more intensive Rayleigh scattering in the UV. How large the difference between UV and visible peak values is then depends on the exact location of the plume within the light paths. If the plume is close to the instrument and completely covered by the shorter UV path, one will get higher values in the UV since the part of the light path probing the higher  $\text{NO}_2$  values has a larger relative contribution to the signal than for the longer visible path. If the plume is further away from the instrument and only in the visible path or close to the UV scattering point, one will retrieve a higher volume mixing ratio in the visible. This relationship contains information on the horizontal distribution of the absorber and will be further investigated in a second manuscript.

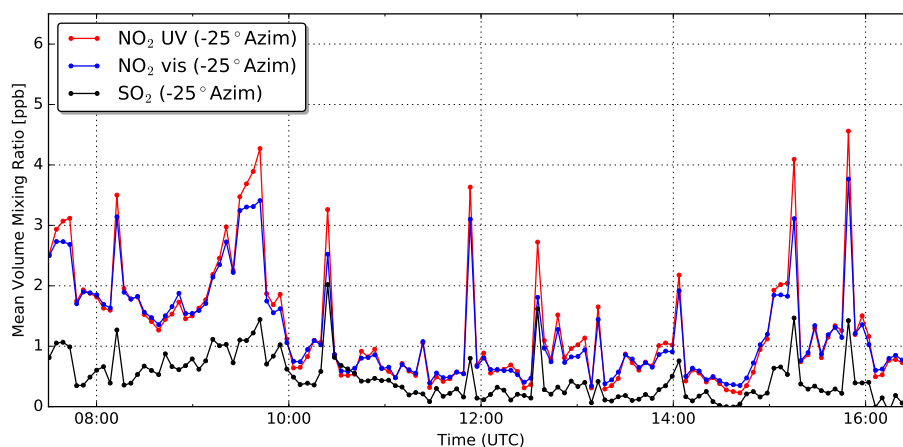


Figure 8: NO<sub>2</sub> (UV and visible) and SO<sub>2</sub> path-averaged volume mixing ratios measured in 0° elevation angle and −25° viewing azimuth angle (approximately NNW direction) on Neuwerk on Wednesday, 23 July 2014.

### 505 4.3 Statistical evaluation of the approach

To investigate quantitatively the relationship between the NO<sub>2</sub> slant column densities measured simultaneously in the UV and visible spectral range, all single pairs of simultaneous measurements are plotted into a scatter plot, shown in the left subplot in the upper row of Fig. (9).

As can be seen from the figure, both measurements are strongly positively correlated with a Pearson correlation coefficient of 0.983. Because of the difference in the horizontal light path lengths in both spectral regions (due to more intense Rayleigh scattering in the UV), the slope of the regression line is 1.30 corresponding to a 30% longer light path in the visible. The intercept of the regression line is small. The right subplot in the upper row of Fig. (9) shows a histogram of the ratios between both slant column densities. The distribution peaks for ratios of 1.3, in good agreement with the retrieved slope from the scatter plot.

When converting the slant column densities to mixing ratios using the O<sub>4</sub> columns, the dependence on light path should be removed and quantitative agreement is expected between the UV and visible retrievals. A scatter plot for the horizontal path averaged volume mixing ratios is shown in the left subplot in the bottom row of Fig. (9). It is clearly visible that the points scatter symmetrically along the 1:1 identity line. Comparing this plot with the plot directly above for the differential slant columns shows that the difference in light path lengths is in fact corrected for by the approach (using the O<sub>4</sub> DSCD as a tracer for the path length). The slope of the regression line is close to 1 and the intercept is very small. The Pearson correlation coefficient has further increased to 0.984. The histogram (right plot) peaks close to one.

As discussed above, differences are still expected not only as a result of measurement uncertainties but also due to different averaging volumes in case of inhomogeneous NO<sub>2</sub> distributions (which is especially the case for ship plumes under certain wind directions). For the horizontal light path lengths, a mean value of 9.3 km with a standard deviation of 2.3 km was retrieved in the UV, and a mean value of 12.9 km with a standard deviation of 4.5 km was retrieved in the visible. On days with optimal measurement conditions (clear sky days), typical horizontal light paths are around 10 km in the UV and 15 km in the visible spectral range.

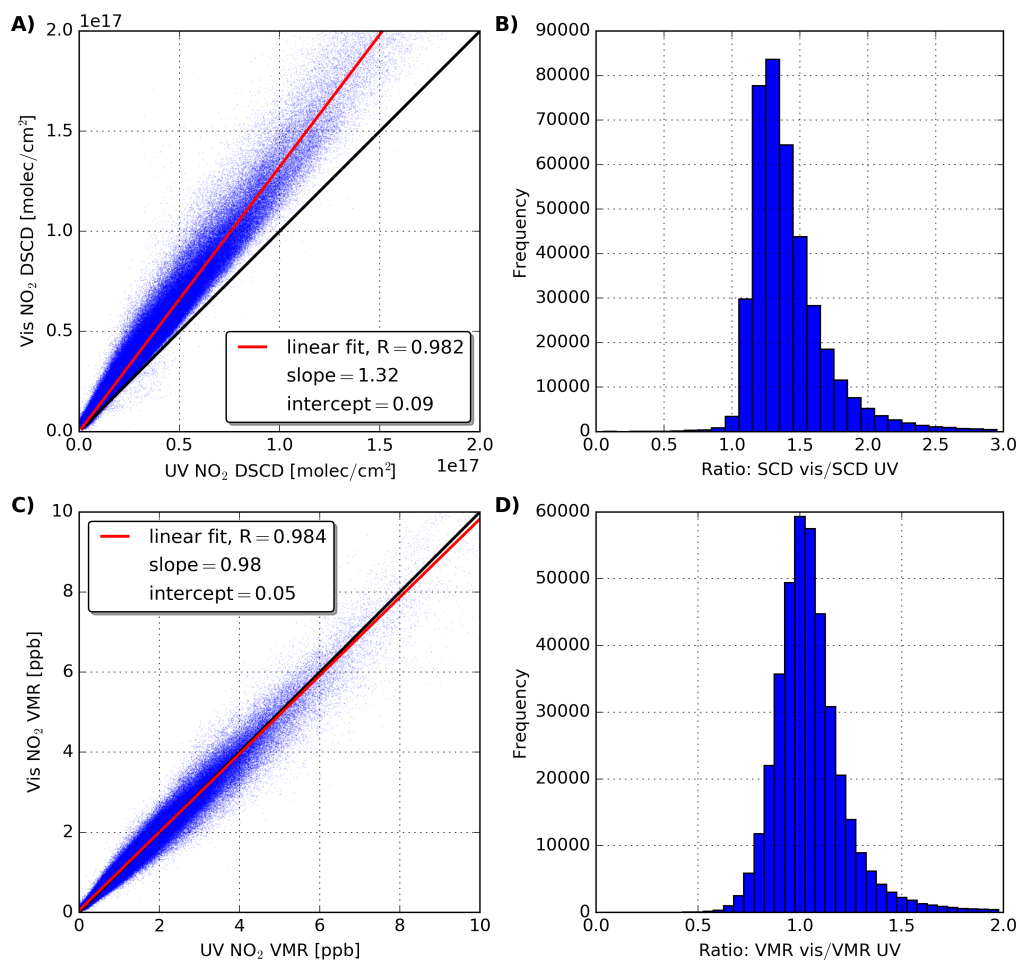


Figure 9: **A)** Scatter plot: NO<sub>2</sub> slant column density retrieved in the visible vs. UV measured in all azimuth angles at 0° elevation for solar zenith angles smaller than 75°. The Pearson correlation coefficient is 0.982. The linear fit was calculated via orthogonal distance regression (Deming regression) and has a slope of 1.33 and an intercept of 0.09. **B)** Histogram of the ratio of the two NO<sub>2</sub> slant column densities (visible/UV). **C)** As A, but for volume mixing ratios. The Pearson correlation coefficient increased to 0.984. The linear fit has a slope of 0.98 and an intercept of 0.05. **D)** Histogram of the ratio of the two NO<sub>2</sub> volume mixing ratios (visible/UV).



535 The horizontal light path lengths retrieved in this study are lower than those retrieved in previous studies with the same approach applied on mountains. Schreier et al. (2016) retrieved a mean horizontal path length of 19 km in the UV for measurements on the German mountain Zugspitze (2650 m a.s.l., and 34 km on the Pico Espejo mountain (4765 m a.s.l.) in Venezuela. However, these sites at very high altitudes are located in a much cleaner surrounding atmosphere, with significantly lower aerosol concentrations and therefore much lower scattering probabilities. This should lead to much longer mean free path lengths between scattering events and longer horizontal light paths than on Neuwerk.

#### 540 4.4 Allocation of ship emission peaks to ships using wind and AIS data

The various information on passing ships transmitted via the *Automatic Identification System* (AIS) and the acquired weather and wind data can be used to allocate the measured pollutant peaks to individual emitting ships.

545 Figure 10, showing measurements from Wednesday, 9 July 2014 contains three sub-plots: The upper one shows the MAX-DOAS differential slant column density of NO<sub>2</sub>. The middle one includes various information about passing ships: The vertical bars indicate when a ship was in the line-of-sight of the MAX-DOAS instrument. Solid bars represent ships coming from the left and going to the right (from west to east, i.e. sailing into the river Elbe), dashed bars vice versa. The colors of the bars indicate the ship length, with small ships shown in blue and very large ships (>350 m) in red. The  
 550 lower sub-plot displays the wind speed and direction.

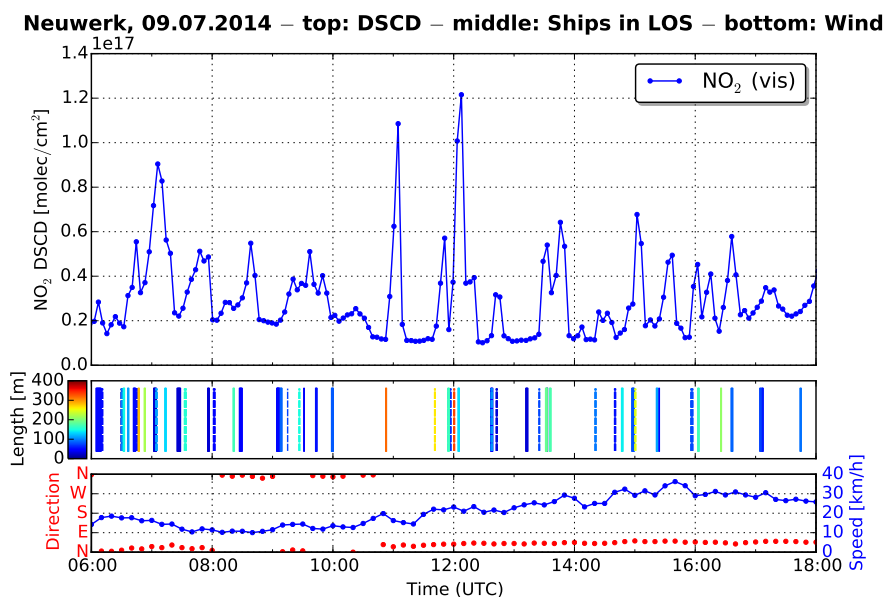


Figure 10: NO<sub>2</sub> DSCD, AIS and wind data for Neuwerk on Wednesday, 9 July 2014.

*Top:* NO<sub>2</sub> differential slant column density (0° elevation, 35° azimuth)

*Middle:* bars indicating that a ship is in the line-of-sight, solid bars: moves from left to right (west to east), dashed vice versa, colors representing ship length

*Bottom:* wind speed and direction measured on Scharhörhörn (HPA)



On this day, the wind was coming from northern directions, directly from the shipping lane, with moderate wind speeds of 10–35 km/h, resulting in low background pollution values ( $1-2 \times 10^{16}$  molecules/cm<sup>2</sup>) as well as sharp and distinct ship emission peaks (up to  $1.2 \times 10^{17}$  molecules/cm<sup>2</sup>) of NO<sub>2</sub>. By comparing the ship emission peak positions to the vertical bars (representing points in time when ships  
555 crossed the MAX-DOAS line-of-sight) in the schematic representation below it can be seen that most of the peaks can be allocated to individual ships. In some cases, when two or more ships simultaneously cross the line-of-sight, the single contributions can not be separated. Large ships (orange and red bars) tend to exhaust more NO<sub>2</sub> while the contribution of small ships (length < 30 m) represented by the dark blue bars is usually not measurable.

#### 560 4.5 Comparison of MAX-DOAS VMR to in-situ measurements

By converting the differential slant column densities to horizontal path averaged volume mixing ratios it is possible to compare the MAX-DOAS measurements to our simultaneous in-situ measurements. For such a comparison, one has to consider the differences of both measurement techniques: The MAX-DOAS averages over a long horizontal light path, while the in-situ device measures at one point  
565 inside the plume. Since ship plumes usually never cover the whole light path but rather a small fraction of it, very high concentration peaks are usually underestimated in the MAX-DOAS VMR. Besides, the peak height in the MAX-DOAS measurements strongly depends on the geometry of plume and line-of-sight of the instrument. If a ship's plume is blown along the line-of-sight, the measured value will be significantly higher than if it is orthogonally crossing the line-of-sight. However, this long light  
570 path is also a major advantage of the MAX-DOAS instrument over the in-situ instrument, since it provides measurements for ship plumes that never hit the radar tower and pass the island in a certain distance or are blown directly away from our instruments.

However, if the pollution is horizontally well-mixed in the measured air mass, which is often the case for background pollution coming from the coast but not for ship plumes, MAX-DOAS and in-situ  
575 instrument should in principle measure the same values.

Figure 11 shows the horizontal path averaged NO<sub>2</sub> volume mixing ratio retrieved from the differential slant column densities shown in Fig. 10 as well as the in-situ NO<sub>2</sub> volume mixing ratio, again in combination with ship data (middle) and wind data (bottom).

From the Figure, it can be easily identified that ship emission peaks measured by the in-situ instru-  
580 ment are both higher and broader than the corresponding MAX-DOAS peaks, leading to a considerably larger integrated peak area, showing nicely the systematic underestimation of the NO<sub>2</sub> concentrations inside ship plumes by the MAX-DOAS instrument due to the averaging along the horizontal light path.

It is also clearly visible, that often a time-shift between MAX-DOAS and in-situ peaks exists, and  
585 that the in-situ peaks are measured with a certain delay. This is due to the long distance of about 6–7 km to the shipping lane, that the plumes have to travel until they reach the radar tower. This time-shift depends on the wind velocity and gets smaller for higher wind speeds. In Figure 11, this dependency can be seen when comparing the magnitude of the time delay for measurements in the morning (low wind speeds) and evening (higher wind speeds).

This travel time also explains the broader peaks in the in-situ measurements, since the emitted  
590 plume spreads and dilutes on its way to the radar tower.

This day of compared MAX-DOAS (visible) and in-situ NO<sub>2</sub> measurements is only a small cutout of three years of measurements on Neuwerk. Longer time-series comparisons for NO<sub>2</sub> (UV) and SO<sub>2</sub> volume mixing ratios are plotted in the upper subplots in Figures 12 and 13.

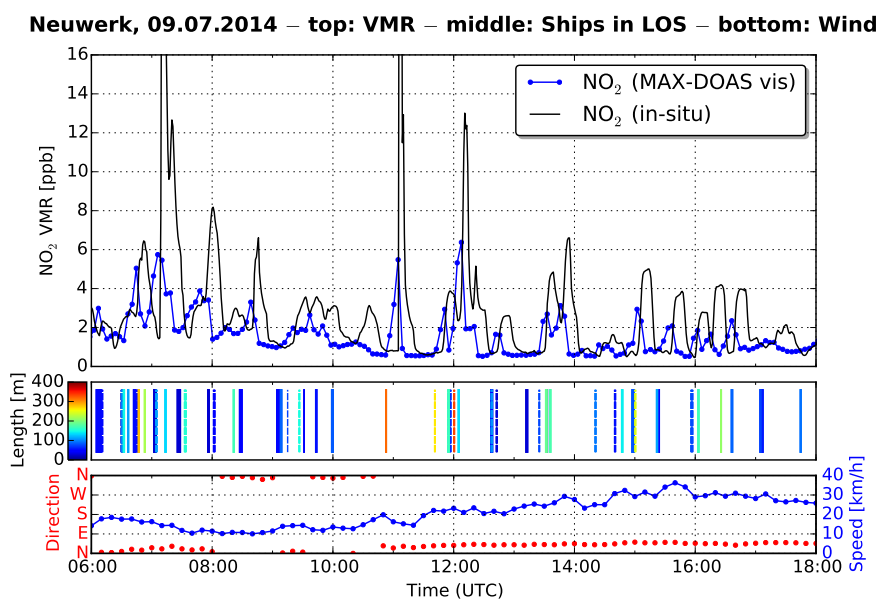


Figure 11: MAX-DOAS and in-situ NO<sub>2</sub> VMR, AIS and wind data on Wednesday, 9 July 2014.  
*Top:* MAX-DOAS (measured in the visible spectral range) and in-situ NO<sub>2</sub> VMR  
*Middle:* bars indicating that a ship is in the line-of-sight, solid bars: moves from left to right (west to east), dashed vice versa, colors representing length  
*Bottom:* wind speed and direction measured on Scharhörn (HPA)



595 Figure 12 shows three months of continuous and simultaneous in-situ and MAX-DOAS (UV) NO<sub>2</sub> measurements in summer 2014. Because of problems with the in-situ SO<sub>2</sub> device from 2014 on mentioned above, for SO<sub>2</sub> a shorter time period with six weeks of measurements from the year before (summer 2013) is shown in Fig. 13.

600 What can be seen from all figures is a good agreement between both instruments for the low values (well-mixed background pollution), but large differences for individual high values (ship emission plumes). During night only the in-situ device can measure, explaining the small, periodically repeated gaps in the MAX-DOAS time-series. Larger gaps are due to instrumental problems linked to power failures.

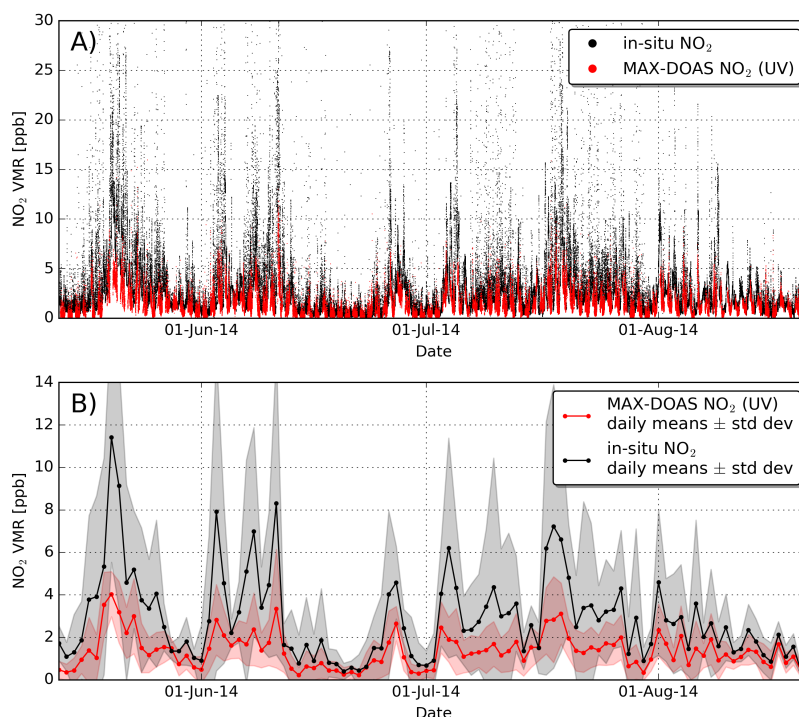


Figure 12: A) Long-term time-series comparison of NO<sub>2</sub> volume mixing ratios from in-situ and MAX-DOAS (UV) instruments during summer 2014. For the MAX-DOAS instrument, all measurements in all azimuth viewing directions are shown.

B) Daily means of NO<sub>2</sub> VMR from MAX-DOAS (UV) and in-situ during summer 2014. For the MAX-DOAS instrument, all measurements in all azimuth viewing directions have been averaged. For the in-situ instrument, the mean of all measurements during the daily MAX-DOAS measurement periods (sunrise till sunset) have been taken.

605 Because of the differences between both measurement techniques and geometries, especially the different height and shape of the peaks as well as the wind speed dependent time-delay due to travel time of plumes, it makes no sense to correlate single measurements. To weaken the impact of those differences, averaging of individual measurements over certain time periods was applied.

610 Figures 12 and 13 show in the lower subplot daily means of the measurement periods presented above. To have comparable conditions, for the in-situ instrument all measurements between the start of the MAX-DOAS measurements in the morning (with sunrise) and the end in the evening (with

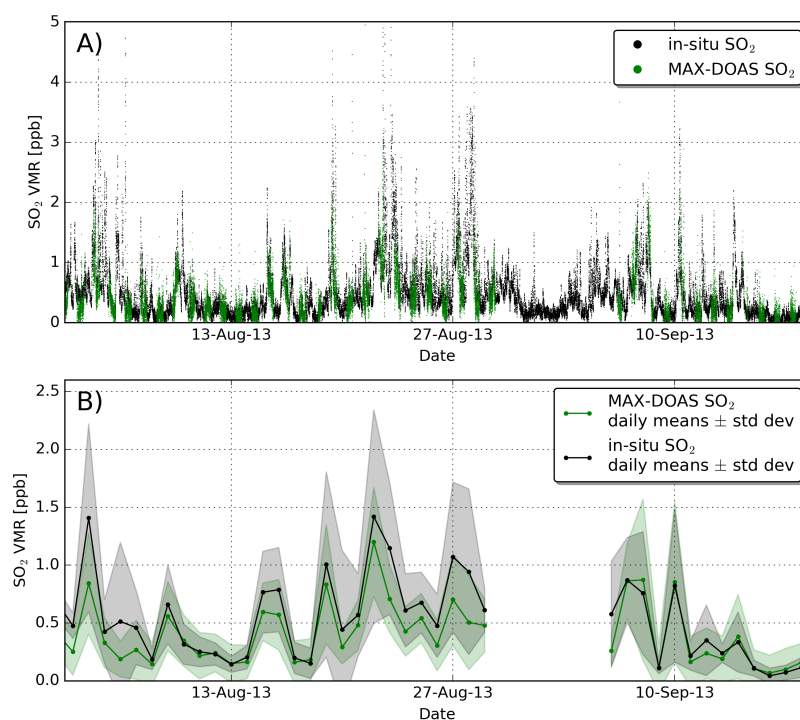


Figure 13: A) Long-term time-series comparison of SO<sub>2</sub> volume mixing ratios from in-situ and MAX-DOAS instruments during summer 2013. For the MAX-DOAS instrument, all measurements in all azimuth viewing directions are shown.

B) Daily means of SO<sub>2</sub> VMR from MAX-DOAS and in-situ during summer 2013. For the MAX-DOAS instrument, all measurements in all azimuth viewing directions have been averaged. For the in-situ instrument, the mean of all measurements during the daily MAX-DOAS measurement periods (sunrise till sunset) have been taken.



sunset) were averaged. The shaded areas show the corresponding standard deviation and indicate the variability during the single days.

As can be seen in the figures, even though in-situ values are usually systematically higher, as expected, a very good agreement of the progression of both curves is found. This illustrates that  
 615 MAX-DOAS can determine day-to-day trends as in-situ measurements.

For the statistical evaluation of the correlation between both instruments, scatter plots for the presented time-series of  $\text{NO}_2$  and  $\text{SO}_2$  are shown in Fig. 14. A clear linear relationship exists between the daily mean measurements of both instruments with only small scatter. Pearson correlation coefficients of 0.87–0.93 prove that both are highly correlated. Using orthogonal distance regression (Deming regression), a linear regression line was fitted to the data. For  $\text{NO}_2$  a slope of  $2.71 \pm 0.16$  (visible) and  $2.72 \pm 0.13$  (UV) was found. For  $\text{SO}_2$  the slope is smaller,  $1.31 \pm 0.09$ . The difference in scaling factors for  $\text{NO}_2$  and  $\text{SO}_2$  is due to a different fraction of shipping emissions on the measured overall emissions and also a different chemistry. During combustion mainly nitric oxide (NO) is produced. This has to be converted to  $\text{NO}_2$  (through reaction with tropospheric ozone) before it can be measured by the  
 625 MAX-DOAS instrument. Since the MAX-DOAS instrument sees the ship plumes in an earlier state, the fraction of  $\text{NO}_2$  should be lower than in the in-situ measurements, explaining at least a part of the difference.

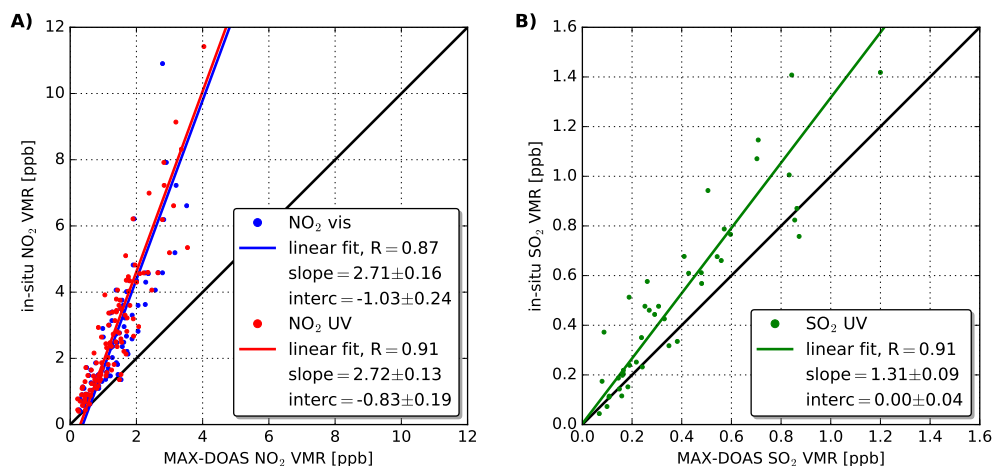


Figure 14: Scatter plot of A)  $\text{NO}_2$  VMR and B)  $\text{SO}_2$  VMR from MAX-DOAS vs. in-situ. For  $\text{NO}_2$  measurements from 2014, for  $\text{SO}_2$  measurements from 2013 are shown. For the MAX-DOAS instrument, to get a better statistic, all measurements in all azimuth viewing directions have been averaged. For the in-situ instrument, the mean of all measurements during the daily MAX-DOAS measurement periods (morning till evening) have been taken.

#### 4.6 Diurnal and weekly variability of $\text{NO}_2$

Although our measurement station is located on a small island in the German Bight close to the  
 630 mouths of the Elbe and Weser river, our measurements are strongly influenced by air pollution from traffic and industry on land, depending on the prevailing wind direction. As can be seen from Fig. 1 A) and 3, wind coming from northeasterly, easterly, southerly and southwesterly directions will blow polluted air masses from the German North Sea Coast and hinterland to Neuwerk. In Figure 15 the diurnal variation of the measured  $\text{NO}_2$  volume mixing ratios is shown as hourly mean values.  
 635 Solid curves show all measurements (for all wind directions), dashed lines show only the subset of



measurements with wind coming from the open North Sea with no coastal background pollution. Looking at the diurnal variation for all measurements, one can see quite nicely the typical daily cycle for road-traffic-influenced air masses with high values in the morning and in the late afternoon during rush hour. If we restrain the data to periods with wind from the open North Sea (dashed curves), this diurnal cycle is gone and values are more or less constant over day and also considerably lower. This result is in accordance with the expectations that the amount of ship traffic should be almost independent from the time of day.

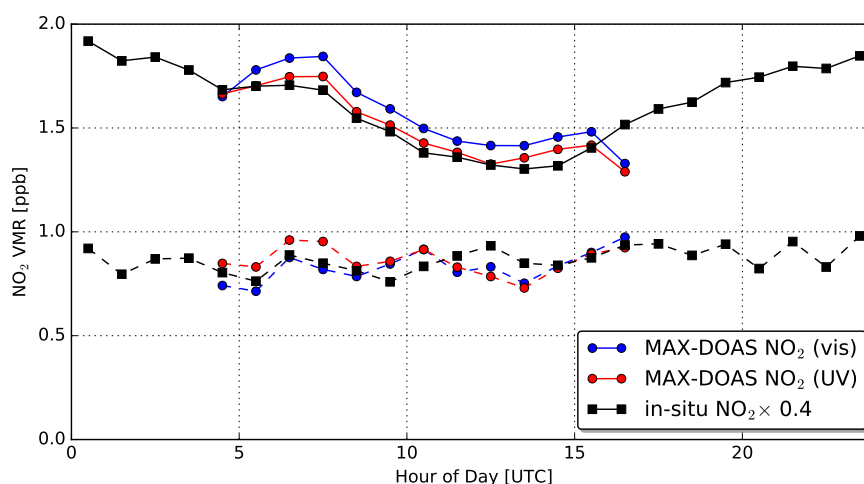


Figure 15: Average diurnal cycles of  $\text{NO}_2$  volume mixing ratios measured with the MAX-DOAS (UV and visible) and in-situ instrument for all wind directions (solid lines) and for north-westerly winds (dashed lines). For a better visual comparability the in-situ values are scaled by a factor of 0.4.

This influence of land-based road traffic is also visible if we take a look at the variability of  $\text{NO}_2$  measurements during the week, as its shown in Fig. 16 as means over the different weekdays. Again solid lines show mean values incorporating all measurements, dashed lines show the averaged subset of measurements with wind coming from northwesterly directions. If we consider the whole time series, lowest values are measured on Sundays, when road traffic is less intense. For wind from the open North Sea, the weekly signal is gone and measurements are more or less constant and again considerably lower. Such a weekly cycle for  $\text{NO}_2$  in polluted regions has been observed and discussed several times before, for example in Beirle et al. (2003), Kaynak et al. (2009), Bell et al. (2009) and Ialongo et al. (2016).

It is also remarkable in these two figures that except for a scaling factor (of approximately 0.4), the progression of the curves retrieved from MAX-DOAS and in-situ measurements show a very good agreement.

The observed difference in  $\text{NO}_2$  mixing ratios between land-influenced and only ship-influenced air masses is in good agreement with a study from Aliabadi et al. (2015). They performed in-situ measurements of gases and particles in the Canadian Arctic in the 2013 shipping season and found 0.7–0.9 ppb (Cape Dorset) and 1.0–1.1 ppb (Resolute, Nunavut) higher  $\text{NO}_x$  concentrations for air masses influenced by local pollution compared to ship-influenced air masses.

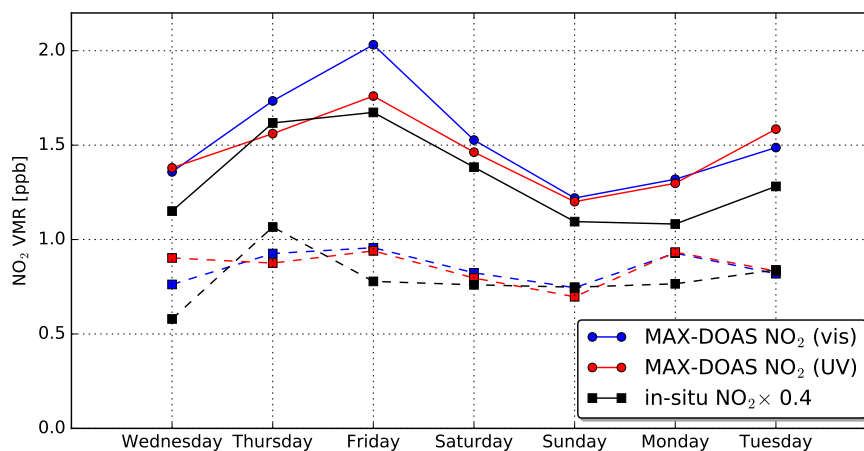


Figure 16: Average weekly cycle of NO<sub>2</sub> volume mixing ratios measured with the MAX-DOAS (UV and visible) and in-situ instrument for all wind directions (solid lines) and for north-westerly winds (dashed lines). For a better visual comparability the in-situ values are scaled by a factor of 0.4.

#### 660 4.7 Dependence of NO<sub>2</sub> and SO<sub>2</sub> pollution levels on wind direction

As already mentioned in Sect. 1, on the 1st of January 2015, the sulfur content of marine fuels allowed inside the North and Baltic Sea Emission Control Areas (ECA) has been substantially decreased from 1.0 % to 0.1 %. Therefore, one would expect lower sulfur dioxide (SO<sub>2</sub>) values in 2015 compared to the years before, especially when the wind is blowing from the open North Sea, where shipping emissions are the only source of SO<sub>2</sub>. This expectation is confirmed by the measurements. Looking at single day measurements (see Fig. 20), no ship emission peaks are visible any more in the 2015 SO<sub>2</sub> data and most of the measured values are within the noise (SO<sub>2</sub> detection limit lies around  $2.5 \times 10^{16}$  mole/cm<sup>2</sup> corresponding to 0.2 ppb for good weather conditions). For a more detailed analysis, mean values over the whole time series before and after 1 January 2015 have been investigated, separated according to the prevailing wind direction.

Two days of SO<sub>2</sub> measurements (20 and 30 October 2014) showing very high values over several hours have been excluded from the time-series. Comparisons with our simultaneous in-situ measurements and measurements from the German Umweltbundesamt at the coast of the North Sea in Westerland/Sylt and at the coast of the Baltic Sea on the island Zingst showing a similar behavior as well as HYSPLIT backward trajectories suggest that on both days SO<sub>2</sub> plumes of the Icelandic volcano Bárðarbunga have influenced the measurements in northern Germany.

Figure 17 shows the wind direction distribution of the mean NO<sub>2</sub> and SO<sub>2</sub> path averaged volume mixing ratios for all measurements before and after the change in fuel sulfur limit regulations.

For SO<sub>2</sub>, a significant decrease is found, particularly for wind directions from West to North with wind from the open North Sea. For this sector, values in 2015 are close to zero. This shows that the new and more restrictive fuel sulfur content limits lead to a clear improvement in coastal air quality. Only for wind from south-southwest there is no change in SO<sub>2</sub>. This might be the influence of emissions from the coal-fired power plant Wilhelmshaven, which is located exactly in this direction.

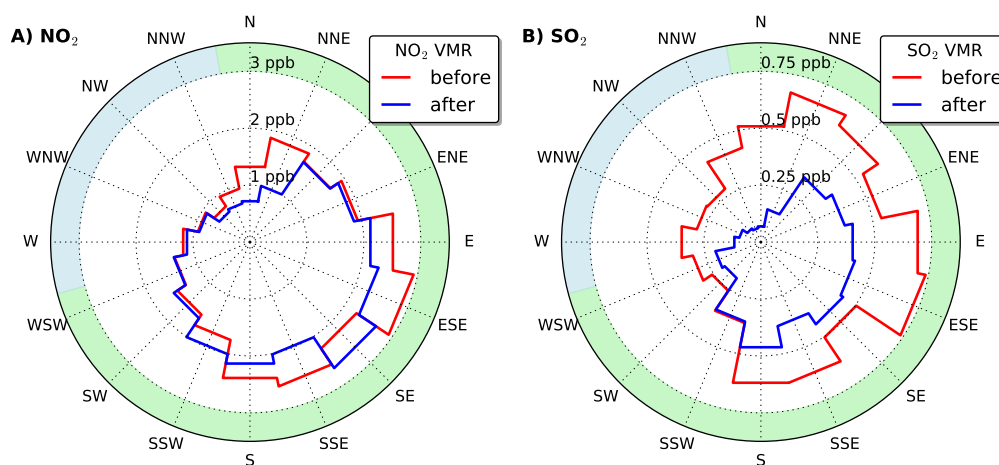


Figure 17: Wind direction distribution of the measured  $\text{SO}_2$  (A) and  $\text{NO}_2$  (B) volume mixing ratio in  $0^\circ$  elevation before and after the change in fuel sulfur limit regulations on 1 January 2015. The colored sectors show directions with wind from the coast (green) and open North Sea (blue).

For  $\text{NO}_2$  on the other hand, both the directional distribution and the absolute values are nearly  
685 identical for both time periods, implying no considerable changes in  $\text{NO}_x$  emissions. This result meets  
the expectations, since no  $\text{NO}_x$  emission limits have been set into force up to now for the North and  
Baltic Sea emission control area.

#### 4.8 Contributions of ships vs. land-based pollution sources on coastal air quality on Neuwerk

690 The distribution of measured  $\text{NO}_2$  and  $\text{SO}_2$  volume mixing ratios depending on the wind direction  
shown in Fig. 17 can be used to estimate the contributions of ships and land-based sources to coastal  
air pollution levels. To trade ship emissions off against land-based emissions (e.g. industry, road  
transport), two representative sectors of wind directions have been chosen, both 90 degrees wide:  
A north-westerly sector ( $258.75^\circ$  to  $348.75^\circ$ ) with wind from the open North Sea and ships as the  
695 only local source of air pollution and a south-easterly sector ( $123.75^\circ$  to  $213.75^\circ$ ) with wind coming  
from land and almost no ship traffic. Air masses brought by wind from the other directions, for  
example from the mouth of the river Elbe in the East of Neuwerk, can contain emissions from land-  
based pollution sources as well as ship emissions. These remaining directions will therefore be called  
"mixed" in the following. It is now assumed, that trace gas concentrations measured during periods  
700 with wind from one of these sectors have their source in the according sector. For getting a good  
statistic, measurements in all azimuth angles have been included. Figure 18 shows the results in  
several pie charts.

For both  $\text{NO}_2$  and  $\text{SO}_2$ , more than half (around 50–60 %) of all measurements have been taken while  
wind was coming from either the assigned sea or land sector. This implies, that not only a small sample,  
705 but the majority of measurements can be used for the estimation of source contributions, making the  
assumption of using these sectors as representative samples for ships and land-based source regions a  
reasonable approximation. There are differences in the time series of  $\text{NO}_2$  and  $\text{SO}_2$  coming from the  
fact that the  $\text{SO}_2$  fit delivers realistic values only up to  $75^\circ$  solar zenith angle and the  $\text{NO}_2$  was fitted  
until  $85^\circ$  SZA, leading to less measurements for  $\text{SO}_2$  than for  $\text{NO}_2$ , especially pronounced in winter



710 times. Despite this, the general distribution pattern of wind direction frequency for NO<sub>2</sub> and SO<sub>2</sub> is quite similar, with wind coming from the sea 32–42 % of the time and from the land sector 18–24 % of the time.

For NO<sub>2</sub> (upper row in Fig. 18), more than half of the total NO<sub>2</sub> measured on Neuwerk can be attributed to wind from either of both sectors, with 21 % coming from ships and 31 % coming from land. This means that from the mean NO<sub>2</sub> level of (1.49 ± 1.30) ppb (mean ± standard deviation) measured on Neuwerk (averaged over all measurements), at least 0.31 ppb is attributed to come from shipping emissions and 0.47 ppb from land-originated sources. The remaining 0.71 ppb is either from ships or coming from the land, or, which is most probable, a mixture of both. The precise shares for this contribution cannot be distinguished from the available data. If we consider only the two sectors, for which we can identify the primary sources and take these as representative, we can say that 40 % of the NO<sub>2</sub> on Neuwerk is coming from shipping emissions, but with 60 %, the majority, is coming from land. One reason for that is that the island Neuwerk is relatively close to the coastline (around 10 km) and is obviously still impacted by polluted air masses from land, which has also been observed in the diurnal and weekly cycle analysis shown in Figures 15 and 16. This might also give us a hint that in coastal regions in Germany land-based sources like road traffic and industry are, despite the heavy ship traffic, the strongest source of air pollution and ship emissions come in second.

For SO<sub>2</sub> the whole time series of measurements from 2013 to 2016 was divided into two periods of nearly the same length: The first period is 2013 and 2014, which was before the introduction of stricter sulfur limits for maritime fuels in the North Sea on 1 January 2015. The according statistics to this period are shown in the middle row in Fig. 18. The second time period, after the change in fuel sulfur limits, includes all measurements from 2015 and 2016, with the corresponding pie plots in the lower row of Fig. 18.

Before the change, 32 % of the measurements were taken when the wind was coming from the sea sector and about 24 % when it was blowing from the dedicated land sector. After the change, the wind was coming a bit more often from sea (42 %) and less often from land (18 %), but in general the situation was quite similar. Although there are certain differences and especially less measurements for SO<sub>2</sub> compared to NO<sub>2</sub>, the wind direction distribution for the whole time series of NO<sub>2</sub> is more or less the average of both periods, like expected.

The contributions of the three sectors (land, sea and mixed) to the total integrated SO<sub>2</sub> with 21 % coming from ships, 29 % from land and 50 % from the mixed sector for the time before the change in sulfur limits are very similar to those of NO<sub>2</sub>, too. After the change, the contribution from the sea sector shrinks significantly from 21 to 7 %, while the contribution from the land sector increased from 29 to 44 %, the contribution from the mixed sector staying the same as around 49 %. That this increase for the land source sector is only a relative increase can be better seen by comparing the absolute contributions: The overall mean SO<sub>2</sub> volume mixing ratio before 2015 is (0.35 ± 0.41) ppb (mean ± standard deviation), to which the sea sector contributed 0.072 ppb and the land sector 0.102 ppb. For 2015 and 2016, the total mean value declined by two-thirds to (0.13 ± 0.31) ppb (mean ± standard deviation). While the contribution from the land sector decreased by 44 % to 0.058 ppb, the contribution from the sea sector (shipping only source) decreased by a factor of 8 to now 0.009 ppb, even though the wind was coincidentally blowing more often from the open sea in this time period. This result shows clearly that the stricter limitations on the fuel sulfur content are working and significantly improved air quality in the North Sea coastal regions with respect to SO<sub>2</sub>. This is in good agreement with other studies such as Kattner et al. (2015), who found that around 95 % of the ships are sticking to the new limits. This implies that the cheaper high sulfur heavy oil fuel is no longer in use in the region of measurement.

If again the two selected sectors are considered as representative for both land and sea sources, the shares of the contributions from sea/land changed from 41 %/59 % (which is very similar to those of NO<sub>2</sub>) to 14 %/86 %. This again shows that since 2015, the vast majority of SO<sub>2</sub> emissions can be



760 attributed to land sources and ships play only a negligible role. Prior to 2015, shipping emissions have  
 761 been a significant source for SO<sub>2</sub> in coastal regions.

762 One aspect which is neglected in this approach is that in situations with good visibility and low  
 763 wind speeds even for wind coming from southern directions, the MAX-DOAS instrument can measure  
 764 ship emissions peaks in the north of the island, but being typically much smaller and less distinct.  
 765 Compared to the often strongly enhanced background pollution in cases with southerly winds, these  
 766 peaks should not play a big roll. This issue will lead to a small overestimation of land sources.

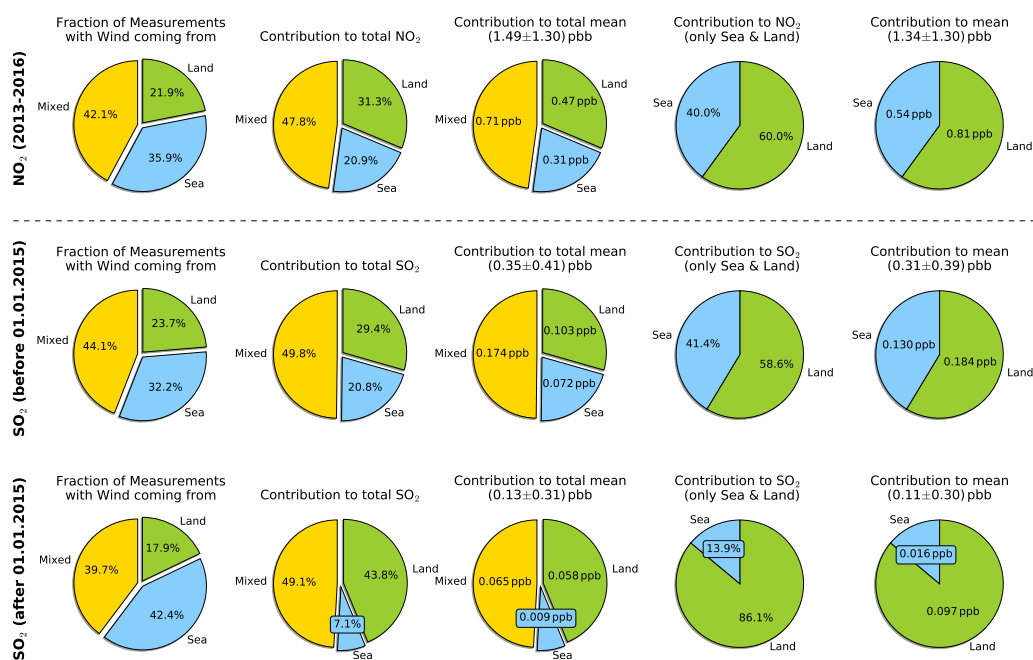


Figure 18: Contributions of ships and land-based pollution sources to measured NO<sub>2</sub> (top row) and SO<sub>2</sub> (middle and bottom row) levels on Neuwerk. For NO<sub>2</sub> the complete time series of measurements from 2013 to 2016 has been taken into account, for SO<sub>2</sub> the data have been divided into the time before and after the change in fuel sulfur content limits. The leftmost statistic shows the percentage of measurements with wind coming only from land (green), only from sea (blue) and from directions with mixed contributions (yellow). The next one to the right shows the contributions to the integrated, total volume mixing ratios from these source regions in percent. The adjacent pie plot shows the contributions to the total mean in ppb. The rightmost pie plots show analogous the percentage and mean VMR contribution by considering only the land and sea sector. It can clearly be seen that the lower fuel sulfur limit lead to a strong decrease in the SO<sub>2</sub> contribution from shipping.

#### 4.9 Determination of SO<sub>2</sub> to NO<sub>2</sub> ratios in ship plumes

For monitoring of pollutant emissions from single ships the individual plume measurement peaks have to be analyzed. It is difficult to derive the absolute amounts (e.g. in mass units) of the emitted gaseous pollutants by our MAX-DOAS remote sensing technique. As explained before, the height and width



770 of the measured peaks does not only depend on the amount of emitted pollutants, but also strongly  
on the geometry, while getting the highest values when measuring alongside the plumes, and much  
smaller values when the plume moves orthogonal to the line-of-sight of our instrument. The result of  
our measurements are integrated concentrations along a long and unknown light path. By using the  
measured  $O_4$  columns as a tracer for the effective light path length as shown above, an approximation  
775 of the horizontal light path length is estimated. With this, long-path averaged volume mixing ratios  
can be calculated. But to get the mixing ratio inside the plume, additional information on the length  
of the light path inside the plume would be needed, which cannot be retrieved from our measurements.  
This means that without further assumptions, we cannot determine emission factors for the emitted  
gases (e.g for emission inventories, which are used as input for model simulations).

780 Although measurements of emission factors cannot be measured by MAX-DOAS directly, both the  
 $NO_2$  and  $SO_2$  signals yield the ratio of both. These ratios can then be compared to ratios of emission  
factors reported in other studies as well as measurements on other sites or with different instruments.

By comparing  $SO_2$  to  $NO_2$  ratios from different ships it is possible to roughly distinguish whether  
a ship is using fuel with high or low sulfur content (giving a high or low  $SO_2$  to  $NO_2$  ratio). The  $SO_2$   
785 to  $NO_2$  ratio can also give insights into the chemistry inside the plumes, since the relative amounts of  
 $NO_2$  and  $NO$  in the emitted  $NO_x$  depend on the time span from stack emission and the presence of  
tropospheric ozone for the conversion of the mainly produced  $NO$  to  $NO_2$ .

From the spectra measured by our MAX-DOAS UV instrument both  $SO_2$  and  $NO_2$  columns can  
be retrieved at once. The two columns are measured at the exact same time along nearly the same  
790 light path. To calculate  $SO_2$  to  $NO_2$  ratios for the measured pollutant peaks simply the ratio of the  
measured differential slant column densities has to be computed.

In order to identify ship related signals, first a running median filter has been applied to the time  
series of  $NO_2$  and  $SO_2$  measurements, to identify low values and to determine the baseline between  
the peaks, which originates from slowly varying well-mixed background pollution levels. The median  
795 filter window (kernel size) was manually adapted for each day. In the next step, by subtracting this  
baseline from the raw signal, one can get rid of the background pollution and only the pollutant peaks  
should remain. A simple peak detection algorithm was used to identify the peaks in the  $NO_2$  signal,  
and then the corresponding peaks in the  $SO_2$  were assigned. This procedure using the  $NO_2$ , which  
peaks are always sharp and distinct, as a tracer for the identification makes it possible to detect the  
800 ship peaks even when the sulfur content in the fuel is very low and almost no  $SO_2$  is measured. In  
the last step, to get a better signal-to-noise ratio, the integrals over both the  $NO_2$  and  $SO_2$  peak are  
calculated and the ratio of both values is computed.

Figure 19 shows the approach as well as the results for one example day in summer 2014, before the  
stricter fuel sulfur content limits were introduced. In both the  $NO_2$  and  $SO_2$  signal high and sharp  
805 peaks are visible, originating from measured ship plumes. The shape of the peaks is also often quite  
similar. The measured  $SO_2$  to  $NO_2$  ratios lie in the range from 0.15 to 0.47 with most of the values  
around 0.3. How different these ratios sometimes are, can nicely be seen from the two ships close to  
12:00 and 12:30 UTC. The first one has a high  $NO_2$  value and a relatively small  $SO_2$  value, the second  
one a lower  $NO_2$  peak and a very high  $SO_2$  peak, indicating that the second ship was using fuel with  
810 a considerably higher sulfur content than the first one.

In contrast to this, Figure 20 shows one example day in summer 2015, after the establishment of  
stricter sulfur limits. For better comparison to Fig. 19, the y-axis limits are the same. Also on this day  
high  $NO_2$  peaks are visible, however, the  $SO_2$  signal shows no clearly distinguishable peaks anymore,  
a result of much less sulfur in the fuel. Consequentially, the measured  $SO_2$  to  $NO_2$  ratios are much  
815 smaller on this day and range from 0.02 to 0.19, with most of them close to 0.1. There might be some  
small peaks in the  $SO_2$  signal, but it cannot be determined if these are real enhancements or just noise  
fluctuations. Because of much less light in the  $SO_2$  fitting window,  $SO_2$  signals are noisier than  $NO_2$ ,



especially when the overall values are small. From this plot one can also see that this method slightly overestimate the SO<sub>2</sub> to NO<sub>2</sub> ratios when no SO<sub>2</sub> peaks can be measured, since the noise also consists of a lot of small peaks, which might be wrongly assigned to SO<sub>2</sub>.

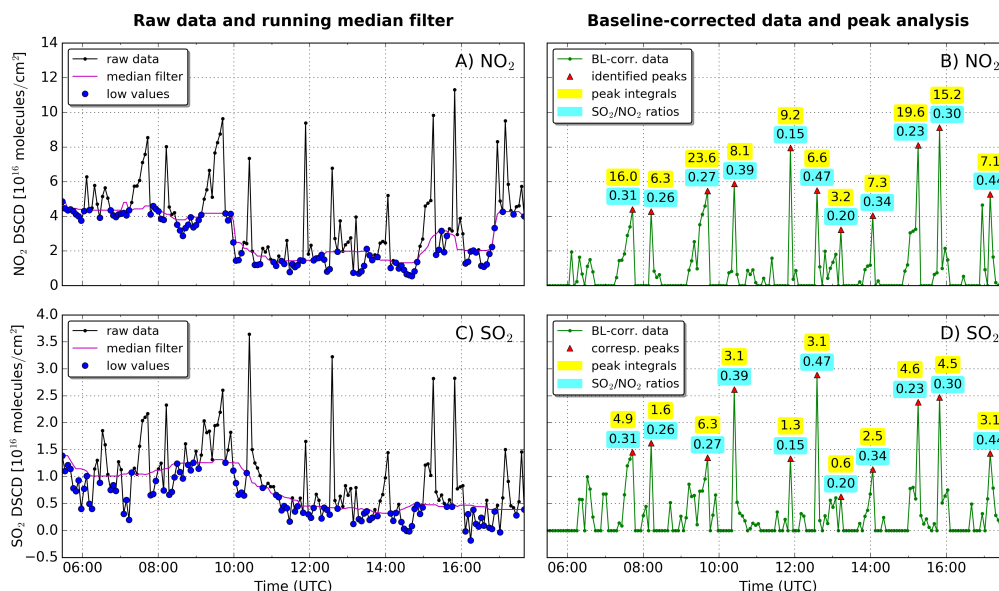


Figure 19: Calculation of SO<sub>2</sub> to NO<sub>2</sub> ratios for ship emission peaks for one example day (23.07.2014) before the change in sulfur emission limits. Subplot A) shows the UV NO<sub>2</sub>-DSCD raw data for 0° elevation and -25° azimuth. A running median filter (over 17 points) is used to determine low NO<sub>2</sub> values for the subtraction of the background NO<sub>2</sub> signal. B) shows the baseline-corrected NO<sub>2</sub> data for which the automatically identified peaks are highlighted with red triangles. Numbers close to the peaks denote the peak integrals in  $1 \times 10^{16}$  molecules/cm<sup>2</sup> (marked in yellow) and the SO<sub>2</sub> to NO<sub>2</sub> ratios (marked in blue). C) and D) show the corresponding plots for SO<sub>2</sub>. For SO<sub>2</sub> a running median kernel size of 29 points has been used.

For a statistically meaningful comparison of both time periods two representative samples of ship emission peaks have been selected by hand for days with good measurement conditions, which were identified by using the solar radiation measurement data of our weather station. One sample of 1060 peaks, measured in 2013 and 2014 representing the state before introduction of stricter fuel sulfur content limits, and another sample of 1060 peaks measured in 2015 and 2016, representing the situation afterwards, were retrieved. It has to be noted that it cannot be ruled out that a certain fraction of ships were measured repeatedly on different days. It is also highly probable that the plume from some individual ships was measured multiple times at different locations in the different azimuth directions while the ship was passing the island.

The distributions of the SO<sub>2</sub> to NO<sub>2</sub> ratios derived from the peak integrals for the two samples are shown in a histogram in Fig. 21. It can be seen that SO<sub>2</sub> to NO<sub>2</sub> ratios were considerably higher before 2015, with a mean of 0.31, a standard deviation of 0.13 and a median value of 0.30. After the change in fuel sulfur content limits, the SO<sub>2</sub> to NO<sub>2</sub> ratios became much lower with a mean of 0.087, a standard deviation of 0.065 and a median value of 0.074, a reduction by a factor of four. A Welch's t-test (unequal variances t-test) gives a p-value of zero (in double-precision floating-point format) indicating that the reduction is statistically highly significant. These results can be compared

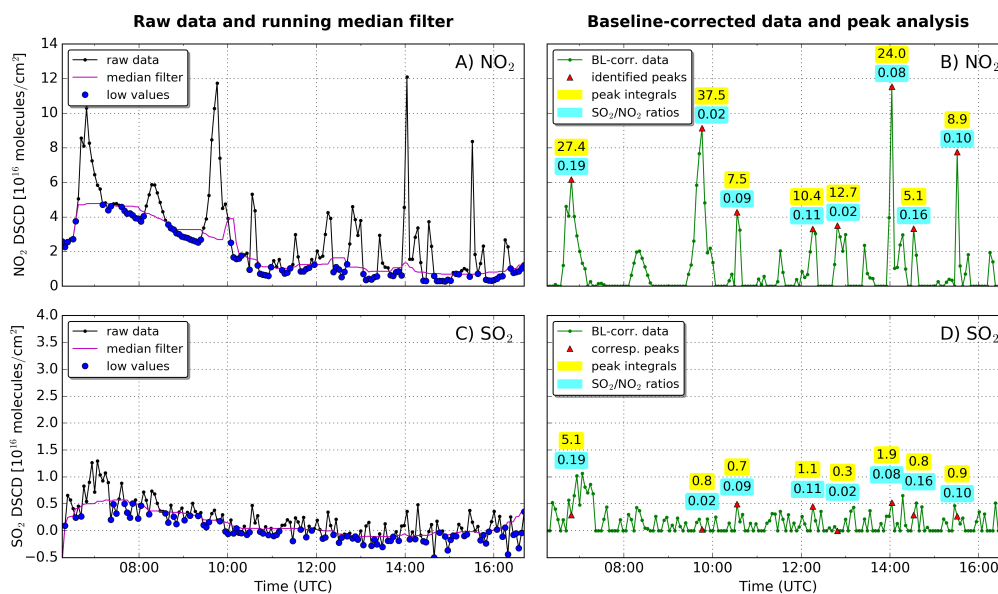


Figure 20: As Figure 19 but for an example day (03.07.2015) after the introduction of stricter fuel sulfur content limits. Measurements in 0° elevation and 65° azimuth are shown. A running median filter over 21 (29) point for NO<sub>2</sub> (SO<sub>2</sub>) has been used. Peak integrals are given in 1 × 10<sup>16</sup> molecules/cm<sup>2</sup>

to the overall average SO<sub>2</sub> to NO<sub>2</sub> ratios on all days with good measurement conditions from which the peaks have been selected: For the time before 2015, this gives a mean value of 0.10 and a median of 0.17 and for 2015 and 2016, one gets a mean value of 0.024 and a median of 0.058. As expected, these values are significantly lower than the SO<sub>2</sub> to NO<sub>2</sub> ratios obtained from the ship plumes which do not include background pollution.

Because the SO<sub>2</sub> noise interference mentioned above leading to overestimation of the ratios for low SO<sub>2</sub> levels, the results for the time period after the reduction in sulfur limits should be considered as upper limits. The reduction is expected to be even more pronounced in reality.

It is also interesting to compare our results with those from other studies. McLaren et al. (2012) measured NO<sub>2</sub> to SO<sub>2</sub> emission ratios in marine vessel plumes in the Strait of Georgia in summer 2005. In a sample of 17 analyzed plumes, a median molar NO<sub>2</sub>/SO<sub>2</sub> ratio of 2.86 was found. Translated into a SO<sub>2</sub>/NO<sub>2</sub> ratio this yields a value of 0.35 which is, considering the small sample size, in good agreement with our findings for the time before 2015.

Another study was carried out from Diesch et al. (2013) measuring gaseous and particulate emissions from various marine vessel types and a total of 139 ships on the banks of the river Elbe in 2011. From their reported SO<sub>2</sub> and NO<sub>2</sub> emission factors one can also derive SO<sub>2</sub> to NO<sub>2</sub> emission ratios: For small ships (<5000 tons) a ratio of 0.13 and an average fuel sulfur content (FSC) of (0.22 ± 0.21) % was found, for medium size ships (5000–30 000 tons) a ratio of 0.24 and a FSC of (0.46 ± 0.40) % and for large ships (>30 000 tons) a ratio of 0.28 and a FSC of (0.55 ± 0.20) %. Especially the values for medium size and large ships fit quite well to our results while plumes from very small vessels (if measurable at all) have often not been taken into account for the statistic because of the low signal-to-noise ratio.

When assuming that their dependence between SO<sub>2</sub> to NO<sub>2</sub> ratio and fuel sulfur content is also



860 applicable to our dataset, we can roughly estimate that the ships measured by us before 2015 used an average sulfur content of 0.5–0.7%, in good agreement with the results of Kattner et al. (2015), which since 2015 decreased to 0.1–0.2% as an upper limit.

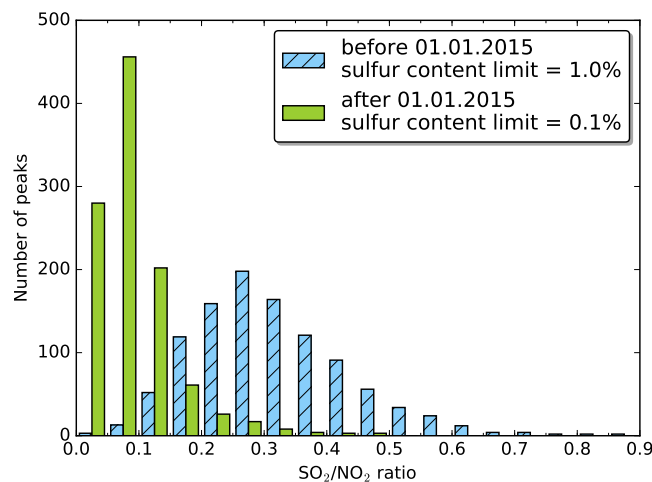


Figure 21: Histogram showing the distribution SO<sub>2</sub> to NO<sub>2</sub> ratios in two samples ( $N = 1060$  for each) of ship emission peaks measured in 0° elevation and all azimuth angles for the time before (blue) and after (green) the change in fuel sulfur content regulation on the 1st of January 2015.

## 5 Summary and conclusions

In this study, three years of MAX-DOAS observations of NO<sub>2</sub> and SO<sub>2</sub> taken on the Island Neuwerk close to the shipping lane towards the harbor of Hamburg, Germany were analyzed for pollution emitted from ships. Using measurements taken at 0° elevation into different azimuthal directions, both background pollution and plumes from individual ships could be identified. Using simultaneously retrieved O<sub>4</sub> columns, path averaged volume mixing ratios for NO<sub>2</sub> and SO<sub>2</sub> could be determined. Comparison of NO<sub>2</sub> measurements in the UV and visible parts of the spectrum showed excellent agreement between mixing ratios determined from the two retrievals, demonstrating consistency in the results.

875 MAX-DOAS measurements were also compared to co-located in-situ observations. High correlation was found between mixing ratios derived with the two methods on average, in-situ measurements showing systematically larger values, in particular during ship emission peaks. This deviations can be understood by the difference in measurement volume, the MAX-DOAS measurements averaging over light paths of several kilometers. For NO<sub>2</sub>, the difference is larger than for SO<sub>2</sub>, probably because of conversion of NO to NO<sub>2</sub> during the transport from the ship where the signal is detected by MAX-DOAS to the measurement site where the in-situ instrument was located.

880 Although the measurement site is within a few kilometers from one of the main shipping lanes, it is also influenced by land based pollution depending on wind direction. Comparing measurements taken under wind direction from the shipping lane and from land, systematic differences in the diurnal and weekly cycles of NO<sub>2</sub> are found. While NO<sub>2</sub> from land shows high values in the morning and evening



and lower values around noon and on weekends, NO<sub>2</sub> levels from sea are more or less constant over time as expected from continuous shipping operations. These results are found in both MAX-DOAS and in-situ observations. Both NO<sub>2</sub> and SO<sub>2</sub> levels are often higher when wind is coming from land, indicating that land based sources contribute significantly to pollution levels on the island in spite of its vicinity to the shipping lanes. Analyzing the wind dependence of the signals in more detail, and excluding data with mixed air mass origin, the contribution of shipping sources to pollution on Neuwerk could be estimated to be 40 % for NO<sub>2</sub> and 41 % for SO<sub>2</sub> in the years 2013 and 2014. As nearly half of the measurements were taken under wind coming from mixed directions, this is only a rough estimate but is still a surprisingly small fraction.

Although the MAX-DOAS measurements cannot be used to directly determine NO<sub>x</sub> or SO<sub>2</sub> emissions from individual ships due to the measurement geometry, the ratio of SO<sub>2</sub> to NO<sub>2</sub> column averaged mixing ratios gives a good estimate of the SO<sub>2</sub> to NO<sub>x</sub> emission ratio. Using the data from Neuwerk, more than 2000 individual ship emission plumes were identified and the ratio of SO<sub>2</sub> to NO<sub>2</sub> computed after subtraction of the background values. The results varied between ships but on average yielded values of about 0.3 for the years 2013/2014, in good agreement with results from other studies.

Since January 2015, much lower fuel sulfur content limits of 0.1 % apply in the North and Baltic Sea. This resulted in large changes in SO<sub>2</sub> levels in the MAX-DOAS measurements when the wind is coming from the shipping lanes. In fact, ship related SO<sub>2</sub> peaks are rarely observed anymore since 2015. Applying the same analysis as for the period before the change in legislation, no significant changes were found for NO<sub>2</sub> in terms of ratio between ship and land contribution or absolute levels. For SO<sub>2</sub> in contrast overall levels were reduced by two-thirds, and the relative contribution of shipping sources was reduced from 41 % to 14 %. It is interesting to note that a reduction in SO<sub>2</sub> levels was also observed in most wind directions coming from land, presumably because shipping emissions also contributed to SO<sub>2</sub> levels in coastal areas.

In summary, long-term measurements of NO<sub>2</sub> and SO<sub>2</sub> using a MAX-DOAS instrument demonstrated the feasibility of monitoring pollution originating from ships remotely. Pollution signals from individual ships can be identified and path averaged mixing ratios be determined, which under background pollution situations agree well with in-situ observations. MAX-DOAS measurements do not provide emission estimates for individual ships but allow statistical analysis of signals from thousands of ships at a distance and even under unfavorable wind conditions. Implementation of stricter sulfur limits in shipping fuel lead to a large reduction in SO<sub>2</sub>/NO<sub>x</sub> ratios in shipping emissions and a significant reduction in SO<sub>2</sub> levels at the German coast. The amounts of NO<sub>2</sub> are as expected not significantly impacted by the change of sulfur content in the fuel. This implies that combustion temperatures were probably not significantly changed. The overall contribution of ship emissions to pollution levels at the measurement site is large but land based sources still dominate, even in the immediate vicinity of shipping lanes.

## Acknowledgements

The research project which facilitated the reported study was funded in part by the German Federal Maritime and Hydrographic Agency (Bundesamt für Seeschifffahrt und Hydrographie, BSH) and the University of Bremen. The authors thank the Waterways and Shipping Office Cuxhaven (Wasser- und Schifffahrtsamt, WSA) and the Hamburg Port Authority (HPA) for their help and support.



## References

- Alföldy, B., Lööv, J. B., Lagler, F., Mellqvist, J., Berg, N., Beecken, J., Weststrate, H., Duyzer, J.,  
 925 Bencs, L., Horemans, B., Cavalli, F., Putaud, J. P., Janssens-Maenhout, G., Csordás, A. P., Van  
 Grieken, R., Borowiak, A., and Hjorth, J. (2013). “Measurements of air pollution emission factors  
 for marine transportation in SECA”. In: *Atmospheric Measurement Techniques* 6.7, pp. 1777–  
 1791. ISSN: 18671381. DOI: 10.5194/amt-6-1777-2013.
- Aliabadi, A. A., Staebler, R. M., and Sharma, S. (2015). “Air quality monitoring in communities of  
 930 the Canadian Arctic during the high shipping season with a focus on local and marine pollution”.  
 In: *Atmospheric Chemistry and Physics* 15.5, pp. 2651–2673. ISSN: 16807324. DOI: 10.5194/acp-  
 15-2651-2015.
- Aulinger, A., Matthias, V., Zeretzke, M., Bieser, J., Quante, M., and Backes, A. (2016). “The impact of  
 shipping emissions on air pollution in the greater North Sea region – Part 1: Current emissions and  
 935 concentrations”. In: *Atmospheric Chemistry and Physics* 16.2, pp. 739–758. DOI: 10.5194/acp-  
 16-739-2016. URL: <http://www.atmos-chem-phys.net/16/739/2016/>.
- Balzani Lööv, J. M., Alföldy, B., Gast, L. F. L., Hjorth, J., Lagler, F., Mellqvist, J., Beecken, J., Berg,  
 N., Duyzer, J., Weststrate, H., Swart, D. P. J., Berkhout, A. J. C., Jalkanen, J. P., Prata, A. J., Van  
 Der Hoff, G. R., and Borowiak, A. (2014). “Field test of available methods to measure remotely  
 940 SO<sub>x</sub> and NO<sub>x</sub> emissions from ships”. In: *Atmospheric Measurement Techniques* 7.8, pp. 2597–  
 2613. ISSN: 18678548. DOI: 10.5194/amt-7-2597-2014.
- Beecken, J., Mellqvist, J., Salo, K., Ekholm, J., and Jalkanen, J. P. (2014). “Airborne emission measure-  
 ments of SO<sub>2</sub>, NO<sub>x</sub> and particles from individual ships using a sniffer technique”. In: *Atmospheric  
 Measurement Techniques* 7.7, pp. 1957–1968. ISSN: 18678548. DOI: 10.5194/amt-7-1957-2014.
- 945 Beecken, J., Mellqvist, J., Salo, K., Ekholm, J., Jalkanen, J. P., Johansson, L., Litvinenko, V., Volodin,  
 K., and Frank-Kamenetsky, D. A. (2015). “Emission factors of SO<sub>2</sub>, NO<sub>x</sub> and particles from ships  
 in Neva Bay from ground-based and helicopter-borne measurements and AIS-based modeling”.  
 In: *Atmospheric Chemistry and Physics* 15.9, pp. 5229–5241. ISSN: 16807324. DOI: 10.5194/acp-  
 15-5229-2015.
- 950 Beirle, S., Platt, U., Glasow, R. von, Wenig, M., and Wagner, T. (2004). “Estimate of nitrogen oxide  
 emissions from shipping by satellite remote sensing”. In: *Geophysical Research Letters* 31.18, pp. 4–  
 7. ISSN: 00948276. DOI: 10.1029/2004GL020312.
- Beirle, S., Platt, U., Wenig, M., and Wagner, T. (2003). “Weekly cycle of NO<sub>2</sub> by GOME mea-  
 surements: a signature of anthropogenic sources”. In: *Atmospheric Chemistry and Physics* 3.2,  
 955 pp. 2225–2232. ISSN: 16807324. DOI: 10.5194/acpd-3-3451-2003.
- Bell, T. L., Rosenfeld, D., and Kim, K. M. (2009). “Weekly cycle of lightning: Evidence of storm  
 invigoration by pollution”. In: *Geophysical Research Letters* 36.23, pp. 1–5. ISSN: 00948276. DOI:  
 10.1029/2009GL040915.
- Berg, N., Mellqvist, J., Jalkanen, J. P., and Balzani, J. (2012). “Ship emissions of SO<sub>2</sub> and NO<sub>2</sub>:  
 960 DOAS measurements from airborne platforms”. In: *Atmospheric Measurement Techniques* 5.5,  
 pp. 1085–1098. ISSN: 18671381. DOI: 10.5194/amt-5-1085-2012.
- Bobrowski, N. and Platt, U. (2007). “SO<sub>2</sub>/BrO ratios studied in five volcanic plumes”. In: *Journal  
 of Volcanology and Geothermal Research* 166.3-4, pp. 147–160. ISSN: 03770273. DOI: 10.1016/j.  
 jvolgeores.2007.07.003.
- 965 Bogumil, K., Orphal, J., Homann, T., Voigt, S., Spietz, P., Fleischmann, O. C., Vogel, A., Hartmann,  
 M., Kromminga, H., Bovensmann, H., Frerick, J., and Burrows, J. P. (2003). “Measurements of  
 molecular absorption spectra with the SCIAMACHY pre-flight model: instrument characterization  
 and reference data for atmospheric remote-sensing in the 230–2380 nm region”. In: *Journal of  
 Photochemistry and Photobiology A: Chemistry* 157.2-3, pp. 167–184. ISSN: 10106030. DOI: 10.  
 970 1016/S1010-6030(03)00062-5. URL: [http://linkinghub.elsevier.com/retrieve/pii/  
 S1010603003000625](http://linkinghub.elsevier.com/retrieve/pii/S1010603003000625).



- 975 Bollmann, M., Bosch, T. (K.), Colijn, F. (K.), Ebinghaus, R. (R. C.), Körtzinger, A. (I. o. M. S.), Latif, M. (I. o. M. S.), Matthiessen, B. (I. o. M. S.), Melzner, F. (I. o. M. S.), Oschlies, A. (I. o. M. S.), Petersen, S. (I. o. M. S.), Proelß, A. (I. o. M. S.), Quaas, M., Requate, T., Reusch, T., Rosenstiel, P., Schrottke, K., Sichelschmidt, H., Siebert, U., Soltwedel, R., Sommer, U., Stattegger, K., Sterr, H., Sturm, R., Treude, T., Vafeidis, A., Bernem, C. van, Beusekom, J. van, Visbeck, M., Wahl, M., Wallmann, K., and Weinberger, F. (2010). “Living With the Oceans”. In: *World Ocean Review: Living with the oceans* 1, p. 236.
- 980 Brasseur, G. P. (1999). *Atmospheric chemistry and global change: [a textbook prepared by scientists at the National Center for Atmospheric Research, Boulder]*. Topics in environmental chemistry. New York, NY [u.a.]: Oxford Univ. Press. ISBN: 0195105214.
- 985 Chen, G., Huey, L. G., Trainer, M., Nicks, D., Corbett, J., Ryerson, T., Parrish, D., Neuman, J. A., Nowak, J., Tanner, D., Holloway, J., Brock, C., Crawford, J., Olson, J. R., Sullivan, A., Weber, R., Schaufli, S., Donnelly, S., Atlas, E., Roberts, J., Flocke, F., Hübler, G., and Fehsenfeld, F. (2005). “An investigation of the chemistry of ship emission plumes during ITCT 2002”. In: *Journal of Geophysical Research D: Atmospheres* 110.10, pp. 1–15. ISSN: 01480227. DOI: 10.1029/2004JD005236.
- 990 Corbett, J. J. and Koehler, H. W. (2003). “Updated emissions from ocean shipping”. In: *Journal of Geophysical Research* 108.D20, p. 4650. ISSN: 0148-0227. DOI: 10.1029/2003JD003751. URL: <http://doi.wiley.com/10.1029/2003JD003751>.
- Corbett, J. J., Fischbeck, P. S., and Pandis, S. N. (1999). “Global nitrogen and sulfur inventories for oceangoing ships”. In: *Journal of Geophysical Research* 104.D3, pp. 3457–3470. ISSN: 0148-0227. DOI: 10.1029/1998JD100040.
- 995 Corbett, J. J., Winebrake, J. J., Green, E. H., Kasibhatla, P., Eyring, V., and Lauer, A. (2007). “Mortality from ship emissions: A global assessment”. In: *Environmental Science and Technology* 41.24, pp. 8512–8518. ISSN: 0013936X. DOI: 10.1021/es071686z.
- 1000 Diesch, J. M., Drewnick, F., Klimach, T., and Borrmann, S. (2013). “Investigation of gaseous and particulate emissions from various marine vessel types measured on the banks of the Elbe in Northern Germany”. In: *Atmospheric Chemistry and Physics* 13.7, pp. 3603–3618. ISSN: 16807316. DOI: 10.5194/acp-13-3603-2013.
- DNV (2008). “Marpol 73/78 Annex VI - Regulations of Air Pollution from Ships - Technical and Operational implications”. In: *Fuel*, pp. 1–32.
- 1005 Endresen, Ø., Sørgard, E., Sundet, J., Dalsøren, S., Isaksen, I., and Berglen, T. (2003). “Emission from international sea transportation and environmental impact”. In: *Journal of Geophysical Research* 108.D17, pp. 1–22. ISSN: 0148-0227. DOI: 10.1029/2002JD002898.
- EU (2005). “Directive 2005/33/EC of the European Parliament and of the Council”. In: *Official Journal of the European Union* 1882, pp. 59–69. DOI: 10.3000/17252555.L\_2009.140.eng. URL: <http://eur-lex.europa.eu/LexUriServ/LexUriServ.do?uri=OJ:L:2005:191:0059:0069:EN:PDF>.
- 1010 — (2008). “Directive 2008/50/EC of the European Parliament and of the Council of 21 May 2008 on ambient air quality and cleaner air for Europe”. In: *Official Journal of the European Communities* 152, pp. 1–43. DOI: <http://eur-lex.europa.eu/LexUriServ/LexUriServ.do?uri=OJ:L:2008:152:0001:0044:EN:PDF>.
- 1015 — (2016). *Air Quality Standards*. URL: <http://ec.europa.eu/environment/air/quality/standards.htm> (visited on 12/15/2016).
- Eyring, V., Bovensmann, H., Cionni, I., Dall’Amico, M., Franke, K., Khlystova, I., Klinger, C., Lauer, A., Paxian, A., Righi, M., and Schreier, M. (2010a). *Impact of Ship Emissions on Atmosphere and Climate, SeaKLIM Final Report*. Tech. rep. DLR, p. 23. URL: [http://www.pa.op.dlr.de/SeaKLIM/SeaKLIM%7B%5C\\_%7DNachwuchsgruppe%7B%5C\\_%7DSchlussbericht%7B%5C\\_%7DFINAL.pdf](http://www.pa.op.dlr.de/SeaKLIM/SeaKLIM%7B%5C_%7DNachwuchsgruppe%7B%5C_%7DSchlussbericht%7B%5C_%7DFINAL.pdf).
- 1020 pdf.



- Eyring, V., Köhler, H. W., Aardenne, J. van, and Lauer, A. (2005a). “Emissions from international shipping: 1. The last 50 years”. In: *Journal of Geophysical Research* 110.D17, p. D17305. ISSN: 0148-0227. DOI: 10.1029/2004JD005619. URL: <http://doi.wiley.com/10.1029/2004JD005619>.
- 1025 Eyring, V., Köhler, H. W., Lauer, A., and Lemper, B. (2005b). “Emissions from international shipping: 2. Impact of future technologies on scenarios until 2050”. In: *Journal of Geophysical Research* 110.D17, p. D17306. ISSN: 0148-0227. DOI: 10.1029/2004JD005620. URL: <http://doi.wiley.com/10.1029/2004JD005620>.
- 1030 Eyring, V., Isaksen, I. S., Berntsen, T., Collins, W. J., Corbett, J. J., Endresen, O., Grainger, R. G., Moldanova, J., Schlager, H., and Stevenson, D. S. (2010b). “Transport impacts on atmosphere and climate: Shipping”. In: *Atmospheric Environment* 44.37, pp. 4735–4771. ISSN: 13522310. DOI: 10.1016/j.atmosenv.2009.04.059. URL: <http://linkinghub.elsevier.com/retrieve/pii/S1352231009003379>.
- 1035 Galle, B., Johansson, M., Rivera, C., Zhang, Y., Kihlman, M., Kern, C., Lehmann, T., Platt, U., Arellano, S., and Hidalgo, S. (2010). “Network for Observation of Volcanic and Atmospheric Change (NOVAC) - A global network for volcanic gas monitoring: Network layout and instrument description”. In: *Journal of Geophysical Research Atmospheres* 115.D5, pp. 1–19. ISSN: 21698996. DOI: 10.1029/2009JD011823.
- 1040 Galloway, J. N., Aber, J. D., Erisman, J. W., Seitzinger, S. P., Howarth, R. W., Cowling, E. B., and Cosby, B. J. (2003). “The Nitrogen Cascade”. In: *American Institute of Biological Sciences* 53.4, p. 341. ISSN: 0006-3568. DOI: 10.1641/0006-3568(2003)053[0341:TNC]2.0.CO;2. arXiv: arXiv:1011.1669v3. URL: <http://www.jstor.org/stable/1314367>.
- 1045 Gomez, L., Navarro-Comas, M., Puentedura, O., Gonzalez, Y., Cuevas, E., and Gil-Ojeda, M. (2014). “Long-path averaged mixing ratios of O<sub>3</sub> and NO<sub>2</sub> in the free troposphere from mountain MAX-DOAS”. In: *Atmospheric Measurement Techniques* 7.10, pp. 3373–3386. ISSN: 18678548. DOI: 10.5194/amt-7-3373-2014.
- Grainger, J. F. and Ring, J. (1962). “Anomalous Fraunhofer Line Profiles”. In: *Nature* 193, p. 762.
- Hönninger, G., Friedeburg, C. von, and Platt, U. (2004). “Multi axis differential optical absorption spectroscopy (MAX-DOAS)”. In: *Atmos. Chem. Phys.* 4, pp. 231–254.
- 1050 Ialongo, I., Hakkarainen, J., Hyttinen, N., Jalkanen, J. P., Johansson, L., Boersma, K. F., Krotkov, N., and Tamminen, J. (2014). “Characterization of OMI tropospheric NO<sub>2</sub> over the Baltic Sea region”. In: *Atmospheric Chemistry and Physics* 14.15, pp. 7795–7805. ISSN: 16807324. DOI: 10.5194/acp-14-7795-2014.
- 1055 Ialongo, I., Herman, J., Krotkov, N., Lamsal, L., Boersma, F., Hovila, J., and Tamminen, J. (2016). “Comparison of OMI NO<sub>2</sub> observations and their seasonal and weekly cycles with ground-based measurements in Helsinki”. In: *Atmospheric Measurement Techniques Discussions* 2, pp. 1–13. ISSN: 1867-8610. DOI: 10.5194/amt-2016-212. URL: <http://www.atmos-meas-tech-discuss.net/amt-2016-212/>.
- 1060 IEA/OECD (2009). *Transport, Energy and CO<sub>2</sub> – moving towards sustainability*. Paris: International Energy Agency. ISBN: 9789264073166.
- International Air Transport Association (IATA) (2015). “IATA Annual Review 2015”. In: p. 62. URL: <http://www.iata.org/about/Documents/iata-annual-review-2015.pdf>.
- 1065 Irie, H., Takashima, H., Kanaya, Y., Boersma, K. F., Gast, L., Wittrock, F., Brunner, D., Zhou, Y., and Van Roozendaal, M. (2011). “Eight-component retrievals from ground-based MAX-DOAS observations”. In: *Atmospheric Measurement Techniques* 4.6, pp. 1027–1044. ISSN: 18671381. DOI: 10.5194/amt-4-1027-2011.
- Jonson, J. E., Tarrason, L., and Bartnicki, J. (2000). *Effects of international shipping on European pollution levels. 2000*. Tech. rep. Oslo, Norway: The Norwegian Meteorological Institute.
- 1070 Kattner, L., Mathieu-Üffing, B., Burrows, J. P., Richter, A., Schmolke, S., Seyler, A., and Wittrock, F. (2015). “Monitoring compliance with sulfur content regulations of shipping fuel by in situ measurements of ship emissions”. In: *Atmospheric Chemistry and Physics* 15.17, pp. 10087–10092.



- ISSN: 1680-7324. DOI: 10.5194/acp-15-10087-2015. URL: <http://www.atmos-chem-phys.net/15/10087/2015/>.
- 1075 Kaynak, B., Hu, Y., Martin, R. V., Sioris, C. E., and Russell, a. G. (2009). “Comparison of weekly cycle of NO<sub>2</sub> satellite retrievals and NO<sub>x</sub> emission inventories for the continental United States”. In: *Journal of Geophysical Research: Atmospheres* 114.5, pp. 1–10. ISSN: 01480227. DOI: 10.1029/2008JD010714.
- 1080 Lack, D. A., Cappa, C. D., Langridge, J., Bahreini, R., Buffaloe, G., Brock, C., Cerully, K., Coffman, D., Hayden, K., Holloway, J., Lerner, B., Massoli, P., Li, S. M., McLaren, R., Middlebrook, A. M., Moore, R., Nenes, A., Nuaaman, I., Onasch, T. B., Peischl, J., Perring, A., Quinn, P. K., Ryerson, T., Schwartz, J. P., Spackman, R., Wofsy, S. C., Worsnop, D., Xiang, B., and Williams, E. (2011). “Impact of fuel quality regulation and speed reductions on shipping emissions: Implications for climate and air quality”. In: *Environmental Science and Technology* 45.20, pp. 9052–9060. ISSN: 0013936X. DOI: 10.1021/es2013424.
- 1085 Lampel, J., Pohler, D., Tschritter, J., Frieß, U., and Platt, U. (2015). “On the relative absorption strengths of water vapour in the blue wavelength range”. In: *Atmospheric Measurement Techniques* 8.10, pp. 4329–4346. ISSN: 18678548. DOI: 10.5194/amt-8-4329-2015.
- 1090 Lauer, a., Eyring, V., Hendricks, J., Jöckel, P., and Lohmann, U. (2007). “Global model simulations of the impact of ocean-going ships on aerosols, clouds, and the radiation budget”. In: *Atmospheric Chemistry and Physics Discussions* 7.4, pp. 9419–9464. ISSN: 1680-7375. DOI: 10.5194/acpd-7-9419-2007.
- Lawrence, M. G. and Crutzen, P. J. (1999). “Influence of NO<sub>x</sub> emissions from ships on tropospheric photochemistry and climate”. In: *Nature* 402.6758, pp. 167–170. ISSN: 0028-0836. DOI: 10.1038/46013.
- 1095 Lee, C., Richter, A., Lee, H., Kim, Y. J., Burrows, J. P., Lee, Y. G., and Choi, B. C. (2008). “Impact of transport of sulfur dioxide from the Asian continent on the air quality over Korea during May 2005”. In: *Atmospheric Environment* 42.7, pp. 1461–1475. ISSN: 13522310. DOI: 10.1016/j.atmosenv.2007.11.006.
- 1100 Masieri, S., Premuda, M., Bortoli, D., Kostadinov, I., Petritoli, A., Ravegnani, F., and Giovanelli, G. (2009). “Cruise ships flow rate emission evaluated by means of a passive DOAS instrument”. In: *SPIE Europe Remote Sensing* 7478, 74781S–74781S–10. DOI: 10.1117/12.830309. URL: <http://dx.doi.org/10.1117/12.830309>.
- 1105 Matthias, V., Auling, A., Backes, A., Bieser, J., Geyer, B., Quante, M., and Zeretzke, M. (2016). “The impact of shipping emissions on air pollution in the greater North Sea region-Part 2: Scenarios for 2030”. In: *Atmospheric Chemistry and Physics* 16.2, pp. 759–776. ISSN: 16807324. DOI: 10.5194/acp-16-759-2016.
- McLaren, R., Wojtal, P., Halla, J. D., Mihele, C., and Brook, J. R. (2012). “A survey of NO<sub>2</sub>:SO<sub>2</sub> emission ratios measured in marine vessel plumes in the Strait of Georgia”. In: *Atmospheric Environment* 46.2, pp. 655–658. ISSN: 13522310. DOI: 10.1016/j.atmosenv.2011.10.044. URL: <http://linkinghub.elsevier.com/retrieve/pii/S135223101101123X>.
- 1110 Meller, R. and Moortgat, G. K. (2000). “Temperature dependence of the absorption cross sections of formaldehyde between 223 and 323 K in the wavelength range 225–375 nm”. In: *Journal of Geophysical Research: Atmospheres* 105.D6, pp. 7089–7101. ISSN: 2156-2202. DOI: 10.1029/1999JD901074. URL: <http://dx.doi.org/10.1029/1999JD901074>.
- 1115 Pandya, R. J., Solomon, G., Kinner, A., and Balmes, J. R. (2002). “Diesel exhaust and asthma: Hypotheses and molecular mechanisms of action”. In: *Environmental Health Perspectives* 110.SUPPL. 1, pp. 103–112. ISSN: 00916765. DOI: 10.1289/ehp.02110s1103.
- 1120 Platt, U. and Perner, D. (1980). “Direct measurements of atmospheric CH<sub>2</sub>O, HNO<sub>2</sub>, O<sub>3</sub>, NO<sub>2</sub>, and SO<sub>2</sub> by differential optical absorption in the near UV”. In: *Journal of Geophysical Research: Oceans* 85.C12, pp. 7453–7458. ISSN: 2156-2202. DOI: 10.1029/JC085iC12p07453. URL: <http://dx.doi.org/10.1029/JC085iC12p07453>.



- Platt, U. and Stutz, J. (2008). *Differential optical absorption spectroscopy*. Physics of Earth and Space Environments. Berlin ; Heidelberg: Springer, XV, 597 S. ISBN: 3-540-21193-4 ; 978-3-540-21193-8 ; 978-3-540-75776-4.
- 1125 Prata, A. J. (2014). “Measuring SO<sub>2</sub> ship emissions with an ultraviolet imaging camera”. In: *Atmospheric Measurement Techniques* 7.5, pp. 1213–1229. ISSN: 18678548. DOI: 10.5194/amt-7-1213-2014.
- Premuda, M., Masieri, S., Bortoli, D., Kostadinov, I., Petritoli, A., and Giovanelli, G. (2011). “Evaluation of vessel emissions in a lagoon area with ground based Multi axis DOAS measurements”. In: *Atmospheric Environment* 45:29, pp. 5212–5219. ISSN: 13522310. DOI: 10.1016/j.atmosenv.2011.05.067. URL: <http://dx.doi.org/10.1016/j.atmosenv.2011.05.067>.
- 1130 Richter, A., Begoin, M., Hilboll, A., and Burrows, J. P. (2011). “An improved NO<sub>2</sub> retrieval for the GOME-2 satellite instrument”. In: *Atmospheric Measurement Techniques* 4.6, pp. 1147–1159. ISSN: 18671381. DOI: 10.5194/amt-4-1147-2011.
- Richter, A. (1997). “Absorptionsspektroskopische Messungen stratosphärischer Spurengase über Bremen, 53° N”. PhD Thesis. Göttingen: Universität Bremen. ISBN: 3897120585.
- 1135 Richter, A., Eyring, V., Burrows, J. P., Bovensmann, H., Lauer, A., Sierk, B., and Crutzen, P. J. (2004). “Satellite measurements of NO<sub>2</sub> from international shipping emissions”. In: *Geophys. Res. Lett.* 31, p. L23110. ISSN: 0094-8276. DOI: 10.1029/2004GL020822.
- Roscoe, H. K., Van Roozendaal, M., Fayt, C., Du Piesanie, A., Abuhassan, N., Adams, C., Akrami, M., Cede, A., Chong, J., Clémer, K., Friess, U., Gil Ojeda, M., Goutail, F., Graves, R., Griesfeller, A., Grossmann, K., Hemerijckx, G., Hendrick, F., Herman, J., Hermans, C., Irie, H., Johnston, P. V., Kanaya, Y., Kreher, K., Leigh, R., Merlaud, A., Mount, G. H., Navarro, M., Oetjen, H., Pazmino, A., Perez-Camacho, M., Peters, E., Pinardi, G., Puentedura, O., Richter, A., Schönhardt, A., Shaiganfar, R., Spinei, E., Strong, K., Takashima, H., Vlemmix, T., Vrekoussis, M., Wagner, T., Wittrock, F., Yela, M., Yilmaz, S., Boersma, F., Hains, J., Kroon, M., Piters, A., and Kim, Y. J. (2010). “Intercomparison of slant column measurements of NO<sub>2</sub> and O<sub>4</sub> by MAX-DOAS and zenith-sky UV and visible spectrometers”. In: *Atmospheric Measurement Techniques* 3.6, pp. 1629–1646. ISSN: 18671381. DOI: 10.5194/amt-3-1629-2010.
- 1140 Rozanov, V. V., Rozanov, A. V., Kokhanovsky, A. A., and Burrows, J. P. (2014). “Radiative transfer through terrestrial atmosphere and ocean: Software package SCIATRAN”. In: *Journal of Quantitative Spectroscopy and Radiative Transfer* 133, pp. 13–71. ISSN: 00224073. DOI: 10.1016/j.jqsrt.2013.07.004. URL: <http://dx.doi.org/10.1016/j.jqsrt.2013.07.004>.
- Schreier, S. F., Richter, A., Wittrock, F., and Burrows, J. P. (2016). “Estimates of free-tropospheric NO<sub>2</sub> and HCHO mixing ratios derived from high-altitude mountain MAX-DOAS observations in the mid-latitudes and tropics”. In: *Atmospheric Chemistry and Physics* 16.5, pp. 2803–2817. ISSN: 16807324. DOI: 10.5194/acp-16-2803-2016.
- 1155 Seinfeld, J. H. and Pandis, S. N. (2006). *Atmospheric chemistry and physics: from air pollution to climate change*. 2. ed. Hoboken, NJ: Wiley. ISBN: 0471720186 and 9780471720188 and 0471720178 and 9780471720171.
- 1160 Serdyuchenko, A., Gorshelev, V., Weber, M., Chehade, W., and Burrows, J. P. (2014). “High spectral resolution ozone absorption cross-sections – Part 2: Temperature dependence”. In: *Atmospheric Measurement Techniques* 7.2, pp. 625–636. ISSN: 1867-8548. DOI: 10.5194/amt-7-625-2014. URL: [http://apps.webofknowledge.com/full%7B%5C\\_%7Drecord.do?product=UA%7B%5C&%7Dsearch%7B%5C\\_%7Dmode=GeneralSearch%7B%5C&%7Dqid=72%7B%5C&%7DSID=4AGMqC1BIln9jo2qV5U%7B%5C&%7Dpage=1%7B%5C&%7Ddoc=2](http://apps.webofknowledge.com/full%7B%5C_%7Drecord.do?product=UA%7B%5C&%7Dsearch%7B%5C_%7Dmode=GeneralSearch%7B%5C&%7Dqid=72%7B%5C&%7DSID=4AGMqC1BIln9jo2qV5U%7B%5C&%7Dpage=1%7B%5C&%7Ddoc=2).
- 1165 Singh, H. B. (1987). “Reactive nitrogen in the troposphere”. In: *Environmental Science & Technology* 21.4, pp. 320–327. ISSN: 0013-936X. DOI: 10.1021/es00158a001.
- Statistische Ämter des Bundes und der Länder (Statistikamt Nord) (2015). *Anzahl der Ankünfte von Kreuzfahrtschiffen im Hamburger Hafen in den Jahren 2005 bis 2014*. URL: <http://de.statista.com/statistik/daten/studie/29729/umfrage/ankuenfte-von-kreuzfahrtschiffen-in-hamburg/>.
- 1170



- Thalman, R. and Volkamer, R. (2013). “Temperature dependent absorption cross-sections of O<sub>2</sub>-O<sub>2</sub> collision pairs between 340 and 630 nm and at atmospherically relevant pressure.” In: *Physical chemistry chemical physics* 15, pp. 15371–15381. ISSN: 1463-9084. DOI: 10.1039/c3cp50968k.
- 1175 URL: <http://www.ncbi.nlm.nih.gov/pubmed/23928555>.
- UNCTAD (2014). *Review of Maritime Transport 2014*, p. 34. ISBN: 9789211128789. URL: [http://unctad.org/en/PublicationsLibrary/rmt2014%7B%5C\\_%7Den.pdf](http://unctad.org/en/PublicationsLibrary/rmt2014%7B%5C_%7Den.pdf).
- (2015). *Review of Maritime Transport 2015*. October. ISBN: 978-92-1-112892-5. URL: [http://unctad.org/en/PublicationsLibrary/rmt2015%7B%5C\\_%7Den.pdf](http://unctad.org/en/PublicationsLibrary/rmt2015%7B%5C_%7Den.pdf).
- 1180 Vandaele, A. C., Hermans, C., Simon, P. C., Roozendael, M. V., Guillemot, J. M., Carleer, M., and Colin, R. (1996). “Fourier Transform Measurement of NO<sub>2</sub> Absorption Cross-Section in the Visible Range at Room Temperature”. In: *J. Atmos. Chem.* 25, pp. 289–305.
- Vinken, G. C. M., Boersma, K. F., Donkelaar, A. van, and Zhang, L. (2014). “Constraints on ship NO<sub>x</sub> emissions in Europe using GEOS-Chem and OMI satellite NO<sub>2</sub> observations”. In: *Atmospheric Chemistry and Physics* 14.3, pp. 1353–1369. ISSN: 1680-7324. DOI: 10.5194/acp-14-1353-2014.
- 1185 URL: <http://www.atmos-chem-phys.net/14/1353/2014/acp-14-1353-2014.html>.
- Wang, T., Hendrick, F., Wang, P., Tang, G., Clémer, K., Yu, H., Fayt, C., Hermans, C., Gielen, C., Müller, J. F., Pinardi, G., Theys, N., Brenot, H., and Van Roozendael, M. (2014). “Evaluation of tropospheric SO<sub>2</sub> retrieved from MAX-DOAS measurements in Xianghe, China”. In: *Atmospheric Chemistry and Physics* 14.20, pp. 11149–11164. ISSN: 16807324. DOI: 10.5194/acp-14-11149-2014.
- 1190 Wayne, R. P. (2006). *Chemistry of atmospheres: an introduction to the chemistry of the atmospheres of earth, the planets, and their satellites*. 3. ed., re. Oxford [u.a.]: Oxford Univ. Press. ISBN: 019850375X and 9780198503750.
- 1195 WHO (2006). *Air Quality Guidelines: Global Update 2005 : Particulate Matter, Ozone, Nitrogen Dioxide, and Sulfur Dioxide*. A EURO Publication. World Health Organization. ISBN: 9789289021920.
- Wittrock, F., Oetjen, H., Richter, A., Fietkau, S., Medeke, T., Rozanov, A., and Burrows, J. P. (2004). “MAX-DOAS measurements of atmospheric trace gases in Ny-Ålesund - Radiative transfer studies and their application”. In: *Atmos. Chem. Phys.* 4, pp. 955–966.
- 1200 WSV (2013). *Verkehr und Güterumschlag*. URL: [http://www.ast-nordwest.gdws.wsv.de/schifffahrt/verkehr%7B%5C\\_%7Dgueterumschlag/index.html](http://www.ast-nordwest.gdws.wsv.de/schifffahrt/verkehr%7B%5C_%7Dgueterumschlag/index.html) (visited on 11/01/2016).
- (2014). *Schiffsverkehr und Güterumschlag*. URL: [http://www.wsd-nord.wsv.de/Schiff-WaStr/Schifffahrt/Schiffsverkehr%7B%5C\\_%7Dund%7B%5C\\_%7Dgueterumschlag/index.html](http://www.wsd-nord.wsv.de/Schiff-WaStr/Schifffahrt/Schiffsverkehr%7B%5C_%7Dund%7B%5C_%7Dgueterumschlag/index.html) (visited on 11/01/2016).
- 1205 Yang, M., Bell, T. G., Hopkins, F. E., and Smyth, T. J. (2016). “Attribution of atmospheric sulfur dioxide over the English Channel to dimethyl sulfide and changing ship emissions”. In: *Atmospheric Chemistry and Physics* 16.8, pp. 4771–4783. ISSN: 16807324. DOI: 10.5194/acp-16-4771-2016.
- Zhang, F., Chen, Y., Tian, C., Lou, D., Li, J., Zhang, G., and Matthias, V. (2016). “Emission factors for gaseous and particulate pollutants from offshore diesel engine vessels in China”. In: *Atmospheric Chemistry and Physics* 16.10, pp. 6319–6334. ISSN: 16807324. DOI: 10.5194/acp-16-6319-2016.
- 1210